Numerical simulations of surface winds and precipitation in Iceland

– Die zweite Aufgabe der theoretischen Meteorologie

Ólafur Rögnvaldsson

Submitted in partial fulfillment
of the Philosophiæ Doctor degree
in meteorology at the
University of Bergen,
Geophysical Institute,
Allégaten 70, 5007 Bergen

November 2012

Contents

List of Figures

List of Tables

Acknowledgements

As this work started in 2002 I must acknowledge the trust and patience I have been shown by the University of Bergen, and in particular Prof. Sigbjørn Grønås. I hope this thesis is a proof that I was worth this trust.

Over the years the projects that make up the bulk of the work presented in this thesis have received financial support from numerous sources. These are:

- RANNÍS (e. the Icelandic Science Fund).
- Tækniþróunarsjóður (e. the Icelandic Innovation Fund).
- Orkusjóður (e. the Icelandic Energy Fund).
- Orkustofnun (e. the National Energy Authority).
- Landsvirkjun.
- Landsnet.
- Orkuveita Reykjavíkur (e. Reykjavík Energy).
- NORA, via the project "Vejrtjeneste for søberedskab", grant number 550-025.
- The Nordic Climate and Energy (CE), Climate, Water and Energy (CWE), and Climate and Energy Systems (CES) research projects and the corresponding Icelandic projects Veður og orka (VO), and Lofthjúpsbreytingar og áhrif þeirra á OrkuKerfi og Samgöngur (LOKS, see http://en.vedur.is/ces).

Working facilities have been provided by the Icelandic Meteorological Office (thanks to Magnús Jónsson), the Hydrological Service of the National Energy Authority (thanks to Árni Snorrason), and in recent years by Iceland GeoSurvey (thanks to Ólafur G. Flóvenz).

The work presented in the first paper was initiated by Tómas Jóhannesson, consequently his responsibility for what has happened since is considerable.

This thesis would not have been accomplished without the tremendous help I have received from my supervisor, Haraldur Ólafsson, especially during the final stage. I'm further indebted to all my co-authors over the years, whom without the papers would obviously never have been written. Many of the figures in chapter 5 were made by my colleague and friend Hálfdán Ágústsson, of which I'm immensely grateful.

I have had the pleasure of meeting and working with many wonderful and talented people during my frequent visits to NOAA/ESRL in Boulder, Colorado. Evelyn, Georg, John, and Sarah, just to name a few (and hopefully not pissing all the others off).

I'm deeply grateful for the time Carlo Casty spent in the shade in June 2011 reading the manuscript and giving me valuable comments and encouragement. Viva my friend.

Thanks to my friend Jian–Wen Bao for re-kindling my passion for science and for all the meaningful (as well as the less meaningful) discussions about life, the universe, and everything over the years. May you enjoy life to the fullest.

Last, but not the least, I'm grateful to my wife María for having walked down the aisle, in spite of my lack of higher education, and for having said yes. The kids are OK too.

This work is dedicated to the loving memory of my father, who taught me to think, and my brother Sigurður, who taught me to think again.

Fyrir mömmu.

Chapter 1

Introduction

1.1 Genesis

In the beginning there was a word, and the word was "application". The reviewers saw that the word was good and so it was accepted. And because of the acceptance of the word, a small company with a big name (Institute for Meteorological Research – IMR) was founded. So begins the tale of many wonders, and even more pages, that eventually will culminate in perhaps the biggest wonder of them all: Yours truly getting a PhD degree in meteorology from the University of Bergen.

Our story begins in 2001 when a project called "Áhrif loftslagsbreytinga á úrkomu og veðurfar á Íslandi" (e. Impacts of climate changes on precipitation and weather in Iceland) was funded by the Icelandic Research Fund (RANNÍS) and was later to form the backbone of this PhD project, which started formally in February 2002, at the University of Bergen. The main purpose of this modest project was to map precipitation in Iceland in the current climate. A secondary goal was to describe possible changes in the precipitation pattern under different climatic conditions. Over the years there have been many side projects and spin-offs from the original project but, most importantly, there has always been a continuity in this work. There have further been many changes in the meteorological research environment in Iceland. Available computational power has increased by orders of magnitude and numerical models have become more advanced. As a consequence the number of end-users for meteorological products and know-how has increased, ranging from local fishermen to to the energy sector through the combination of weather- and runoff models. New development, which is of great importance, happened in early 2012 when IMR launched an on-demand weather forecasting system called SARWeather (Rögnvaldsson, 2011). One of the novelties of SARWEather (short for Search And Rescue Weather) is that it is run on the Amazon EC2 computing cloud. Hence, the need for powerful, and expensive, in-house computing facility is reduced.

On 30 March 2004, IMR started running numerical weather forecasts twice daily for Iceland and its surrounding waters. The model resolution was 9 km with a smaller 3 km resoulution domain covering SW-Iceland. The forecast range was 72 and 24 hours, respectively. Currently, IMR runs model simulations eight times a day for Iceland and various sub-domains in the North-Atlantic. The forecasts range from a day up to a week and the grid resolution is between 1 and 27 km. In addition IMR provides on-demand forecasting service to Iceland Search And Rescue association (ICE-SAR) and the Department of Civil Protection of the Icelandic Police as well as to GDACS – The Global Disaster Alerts and Coordination System. GDACS is a cooperation framework between the United Nations, the European Commission and disaster managers worldwide to improve alerts, information exchange and coordination in the first phase after major sudden-onset disasters.

1.2 Research questions

The subject of this research has mainly been twofold. Firstly, can one use a regional model to dynamically scale down a coarse resolution global atmospheric analysis to gain better understanding of temporal and spatial distribution of winds and precipitation in Iceland? Secondly, and closely related to the first one, what, if anything, is gained by increasing the horizontal resolution of the regional model?

The answer to the first question is of direct economical importance as the geographical distribution of precipitation and winds in Iceland is poorly known but very important for hydrological and wind energy applications, both in general and particularly in the context of climate change. It is also of importance regarding mapping potential wind energy in Iceland, a subject that is gaining increased interest from the local power sector. The answer to the second question relates directly to our ability to forecast winds and precipitation in as much detail as possible, and in so doing helping to save lives and property.

In this thesis new ways to validate numerical simulations of precipitation are presented and tested. Firstly, comparing simulated precipitation to observations of accumulated snow over large ice caps and glaciers. And secondly, using results from numerical model to force a hydrological runoff model. The resulting discharge is then compared to observed discharge from a large number of individual watersheds.

We will also explore the sensitivity of the numerical simulations to a number of parameters, including the growth of hydrometeors, mixing in the atmospheric boundary layer and of the numerical configurations of the models themselves.

1.3 The structure of this work

This thesis is structured as follows: In the next chapter we describe the weather and climate of Iceland in brief. Chapter three deals with the scientific challenges for studies of surface winds and precipitation in Iceland. In this chapter we focus on the availability and quality of observational data. We give a theoretical background to the meteorological processes related to surface winds and precipitation and how these processes are modeled by state of the art atmospheric models. Chapter four contains a short abstract from each of the seven peer reviewed papers presented in this thesis, followed by general discussions in chapter five. Chapter six gives general conclusions followed by discussions of future work in chapter seven. Thereafter, each of the seven research papers is presented in a chronological order.

Chapter 2

Surface winds and precipitation in Iceland

The objectives of this work is to improve our understanding of how the orography of Iceland modifies the impinging atmospheric flow. Especially, how the orography shapes the wind- and precipitation fields. The primary tools chosen for this work have been the MM5 atmospheric model (Grell et al., 1995), and from 2007, the WRF model (Skamarock et al., 2008). Through the study of available observational data and model results a comprehensive and detailed picture of both spatial and temporal distribution of these important variables has emerged.

2.1 Climate and weather in Iceland

Iceland is a mountainous island and is located in the N-Atlantic storm track. Due to this the climate of Iceland is largely governed by the effects orography has on the flow of extra-tropical cyclones. The weather and climate of most parts in Iceland is characterized by strong winds, frequent precipitation, mild winters and relatively cool summers. Mean temperatures are typically close to 0°C in the winter and 10°C in the summer. Annual precipitation varies considerably. In the lowlands in the southern part of Iceland, where orographic effects are not dominating, the mean annual precipitation is about one thousand millimeters but in general less in the north. Although the amplitute of the seasonal cycle is moderate, there can be large fluctuations in the weather on a daily basis. These fluctuations are reflected by the observed weather extremes shown in table 2.1.

The mountains of Iceland contribute to an enhancement of the fluctuations in the weather. The mountains also cause a large spatial variability of both the weather and the climate and they lead to local amplification of weather extremes. The extreme temperatures, precipitation and winds shown in table 2.1 are all enhanced

Table 2.1: *Observed weather extremes from the beginning of instrumental records. Data from Veðurstofa Íslands (e. The Icelandic Meteorological Office).*

Parameter	**Value**	**Location**	**Date**
Min temperature	-38 °C	Möðrudalur & Grímsstaðir, NE-Iceland	22 January 1918
Max temperature	30.5 °C	Teigarhorn, SE-Iceland	22 June 1939
Max 24 hour precipitation	293.3 mm	Kvísker, SE-Iceland	9–10 January 2002
Max one month precipitation	971.5 mm	Kollaleira, E-Iceland	November 2002
Max one year precipitation	4630.4 mm	Kvísker, SE-Iceland	2002
Max ten minute wind speed	62.5 ms^{-1}	Mt. Skálafell, SW-Iceland	20 January 1998
Max wind gust	74.2 ms^{-1}	Mt. Gagnheiði, E-Iceland	16 January 1995
Min sea level pressure	919.7 hPa	Vestmannaeyjar islands, S-Iceland	2 December 1929
Max sea level pressure	1058.5 hPa	Reykjavík, SW-Iceland	3 January 1841

by mountains, either through damming of cold air, warm downslope descent, local acceleration of the airflow or by forced ascending motion as in the Kvísker case of extreme precipitation at the foothills of Mt. Öræfajökull. The fact that the weather in Iceland is to a large extent dominated by synoptic scale weather systems together with the impact of the terrain offers many scientific challenges. As these systems, and their interaction with terrain, can be described quite accurately by present day atmospheric models, this meteorological framework provides conditions where increased spatial resolution in numerical weather prediction models is likely to produce substantial improvements in the quality of local weather forecasts. Furthermore, downscaling of the climate, using limited area models, can give valuable information about spatial and temporal distribution of temperature, precipitation and winds, especially in the data-sparse highlands. The impact of orography on precipitation in the mountains has an economic aspect, since hydraulic power is generated only by water that has fallen as precipitation in the mountains, and not in the lowland. However, most precipitation observations, including long time series,

are from the lowland. Hence, data coverage is poor in the interior and in other high altitude regions.

Chapter 3

Scientifical challenges for studies of surface winds and precipitation in Iceland

3.1 Availability and quality of observational data

Figure 3.1 shows the observational network of weather stations in Iceland. The network consists of stations from Veðurstofa Íslands (e. The Icelandic Meteorological

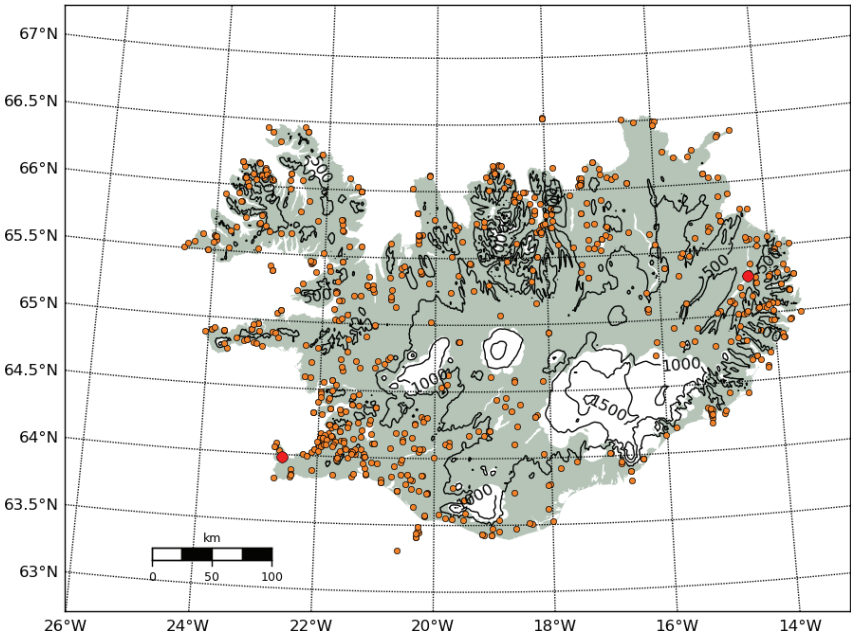

Figure 3.1: *Location of observational stations in Iceland. Rawinsonde stations at Keflavík (SW-Iceland) and Egilstaðir (E-Iceland) airports are marked in red. Contour lines (black) of the terrain are plotted every 500 meters.*

Office), Vegagerðin (e. The Icelandic Road Administration), Landsvirkjun (e. The Icelandic Power Company) and Siglingastofnun (e. The Icelandic Maritime Institute). The observational instruments are fairly homogeneous, except that anenometer height at the Vegagerð stations is around 6 meters and not 10 meters. From the figure it is clear that the bulk of the stations are located in coastal and lowland areas. Upper air observations are only done at two stations, Keflavík airport in SW-Iceland and Egilstaðir airport in E-Iceland, where rawinsondes are released twice a day.

Figure 3.2 shows the location of the operational GPS (e. Global Position System) network run by Háskóli Íslands (e. The University of Iceland), Veðurstofa Íslands, and Landmælingar Íslands (e. The National Land Survey). Only few of these stations provide real-time data and could therefore be used to extract information regarding the vertical profile of water vapor content. As of September 2010, two stations are part of the International GNSS Service network, in Reykjavík and Höfn í Hornafirði. Although observational data from satellites and automatic weather sta-

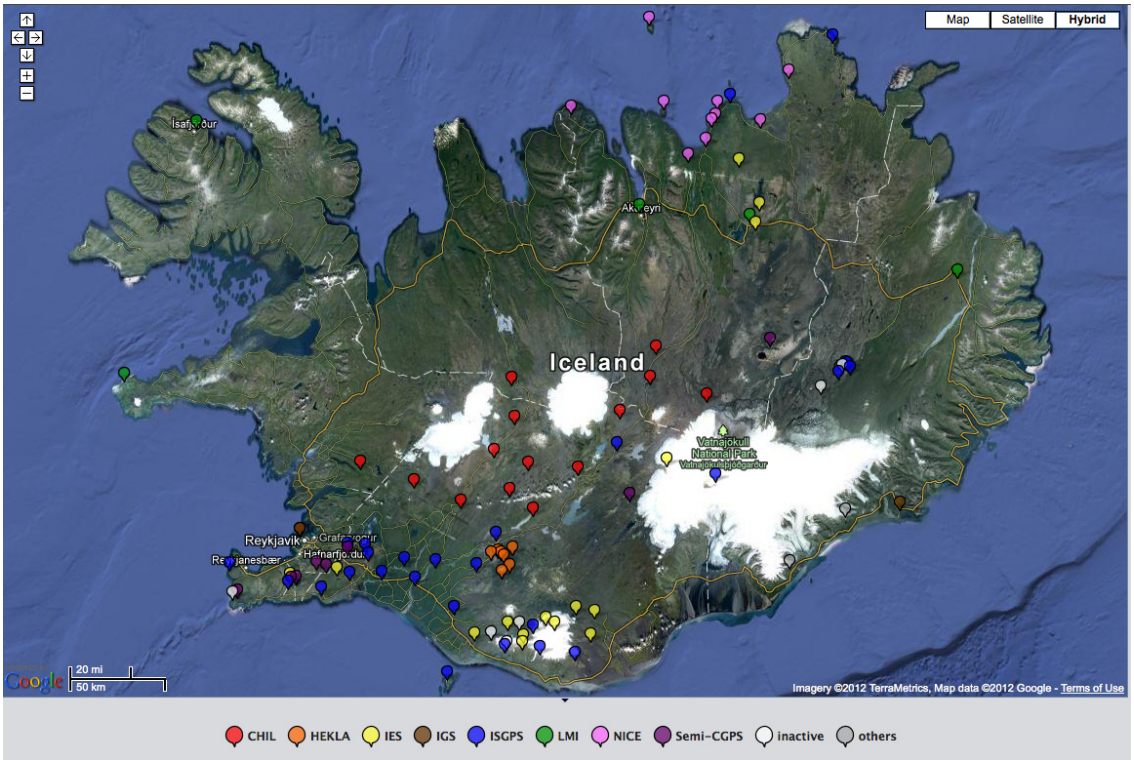

Figure 3.2: *Location of GPS stations in Iceland in November 2012. Figure courtesy of the University of Iceland* [1].

tions is ever increasing there is still a lack of observations throughout the boundary layer and in the interior of Iceland. Without these types of data, it is unclear how

[1] https://notendur.hi.is/runa/cgps.html. Retrieved on 2012-11-08.

much useful information, if any, data assimilation of available surface observations can add to atmospheric analysis from global models like the ECMWF[2] and GFS[3].

3.2 Meteorological processes – Theoretical background

In the late 1940s Charney and Eliassen (1949) showed that topographic Rossby waves, on the horizontal scale of order 10^4 km, seemed to explain the existence of the major 500 hPa trough in the lee of the Himalayas and the Rocky Mountains. This theory is however not applicable to airflow over Iceland, due to its smaller horizontal scale. The reason is that stationary waves only occur when $U = \beta/k^2$. Here U is the wind speed, β is the change in the Coriolis parameter with latitude and k is the zonal wave number. This implies a wavelength given by $L = 2\pi\sqrt{U/\beta}$. With the low β-parameter of Iceland and a typically observed wind speed of 10 m/s this would result in a wavelength of the order 6800 km, which is totally unrealistic for such a narrow "mountain" as Iceland (e.g. Kristjánsson and McInnes (1999)). A more useful approach to understand airflow over and around Iceland would be to use Smith's regime diagram (Smith, 1989).

3.2.1 Smith's theorem

Smith (1989) showed that in order to describe a steady Boussinesq, hydrostatic, non-rotating flow on a free-slip surface, unbounded above for a given mountain shape, one only needs two non-dimensional control parameters. The former is the dimensionless mountain height (also known as the inverse Froude number), $\hat{h} = Nh/U$, where N is the Brunt-Väisälä frequency, h is the mountain height and U is the upstream, horizontal wind. The latter parameter r is the horizontal aspect ratio[4], which must be taken into account to describe the dimensions of the mountain.

3.2.1.1 Flow regimes

There are two phenomena that can alter the kinematic or geometric nature of the flow field. The former is when the flow goes around the mountain instead of over (i.e. flow splitting) and the latter is when wave breaking occurs above the mountain. Each of these begins with the formation of a stagnation point (i.e. a point where

[2] http://www.ecmwf.int

[3] http://www.noaa.gov

[4] $r = a_y/a_x$ where a_x is the cross-mountain width and a_y the along-mountain width. The cross-mountain width is parallel to the upstream wind direction but the along-mountain width is perpendicular to it.

the horizontal wind speed becomes close to zero). For small $\hat{h}$, as is usually the case for small isolated hills, airflow tends to diverge around the hill, but the center streamline (for a hill with left-right symmetry, but some other streamline if the hill shape is complex) is still able to climb over the hill top. For larger hills, a stagnation point can develop on the windward slope. There the center streamline splits and passes around the hill on both sides.

A stagnation point can also form aloft. At such a point $u \ll U$, where U is the main upstream flow speed, the streamline becomes steeply sloping and overturning may follow (Smith, 1989).

3.2.1.2 Regime diagrams

Figure 3.3 summarizes the onset of stagnation as a function of the horizontal aspect ratio r of the mountain and the dimensionless mountain height $\hat{h}$. Note that there are no vertical variations in the upstream values of U and N. The diagram should be used by fixing a value of r and increasing $\hat{h}$ from a small value to a larger one until one of the critical curves is met. If curve A is met first, stagnation begins aloft. If curve B is met first, stagnation begins on the windward slope.

It can be seen that stagnation begins aloft (curve A) for mountain ridges with a large aspect ratio, $r > 1$. Curve B (small dotted line) above curve A should not be taken too seriously since the influence of wave breaking is not taken into consideration in linear theory (Smith, 1989). For a small aspect ratio, $r < 1$, stagnation begins on the windward side of the mountain (curve B). We can now construct three regimes for hydrostatic flow:

1. Below the critical curves, gravity waves propagate vertically and there is neither any flow blocking nor wave breaking.

2. Above curve A (large r), wave breaking occurs.

3. Above curve B (large $\hat{h}$ and small r), stagnation at the surface leads to flow splitting.

A weakness in Smith's theory is that it is both inviscid and irrotational,[5] and unlike in nature, the vertical profiles of wind and stability are uniform. According to Ólafsson and Bougeault (1997) the combined effect of rotation and friction will actually lead to an extension of linear theory resulting in that the qualitative results of Smith's theory should still apply for flow with rotation and friction. Ólafsson (2000) extended Smith's regime diagram by taking into account the effects of rotation and surface friction. His results are depicted in figure 3.4. It is interesting to note that the flow is considerably simpler now. Stagnation aloft does not occur and the flow

[5] It is irrotational in the sense that the Coriolis "force" is absent.

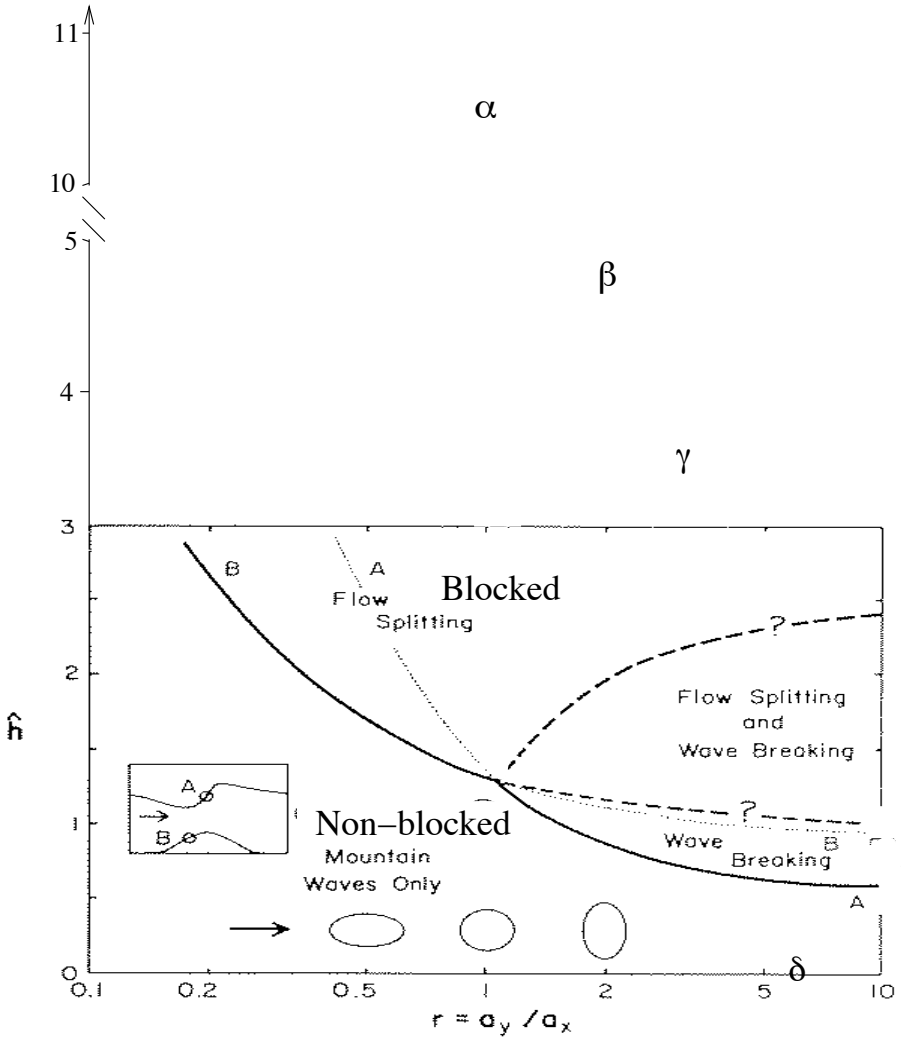

Figure 3.3: *Regime diagram for hydrostatic flow over a mountain. The diagram axes describe the horizontal aspect ratio, r, and the non-dimensional mountain height, $\hat{h}$. Solid curves A and B are linear theory estimates of flow stagnation, suggesting where wave breaking aloft (curve A) and flow splitting (curve B) will begin as $\hat{h}$ increases. Other regime boundaries above the A and B curves (dashed lines) are not yet known. Adapted and redrawn from Smith (1989).*

is simply either blocked or not blocked. It should be emphasized that this is only valid for an atmosphere where both U and N are constant with height. The effects of rotation on the flow are typically described by the non-dimensional Rossby number, *Ro*, defined as U/fL, were U is the mean windspeed, f is the Coriolis parameter and L is the mountain length scale. The Rossby number is a measure of the relative importance of the Coriolis term in the momentum equations. For Iceland it is in order to assume $L = 300$km, $U = 10\text{ms}^{-1}$ and $f = 10^{-4}\text{s}^{-1}$ resulting in a Rossby

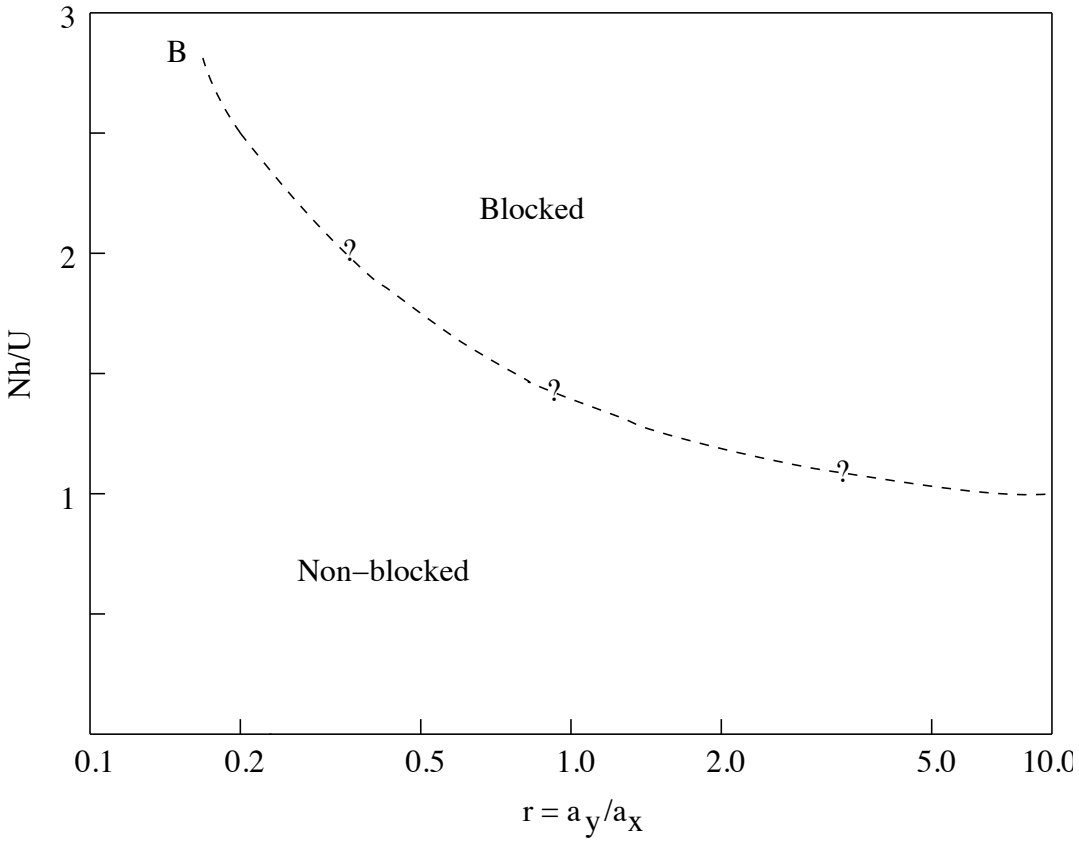

Figure 3.4: *Extension of Smith's regime diagram, where the effects of rotation and surface friction are taken into account. Note that stagnation aloft (curve A in figure 3.3) does not occur anymore. Question marks indicate that the exact position of the line is not known. Adapted and redrawn from Ólafsson (2000).*

number close to 1/3. At that value, the Coriolis force is important, but the flow is not geostrophic. As the length scale is reduced as to represent individual mountain ranges and mountains, the Rossby number increases and the flow becomes less and less affected by the rotation.

The combined effects of the Rossby number (Ro) and the inverse Froude number (Nh/U) on the atmospheric flow is shown in Fig. 3.5. The diagramme shows schematically the patterns of speed-up and slow-down of flow in the vicinity of mountains as a function of the governing non-dimensional numbers, Nh/U and Ro. The upper part of the diagramme represents flow at high Rossby numbers (Ro), where the Coriolis force plays a minor role. At low values of Nh/U, the flow is able to overcome the potential barrier of the mountain. The maximum wind speed is at the top of the mountain (hill), but there is relatively little horizontal variability in the wind speed. At high values of Nh/U, the flow is blocked on the upstream side and it is deflected on each side of it. In this type of flow, the flow speed is significantly reduced both inside a so-called upstream blocking as well as in a wake, downstream

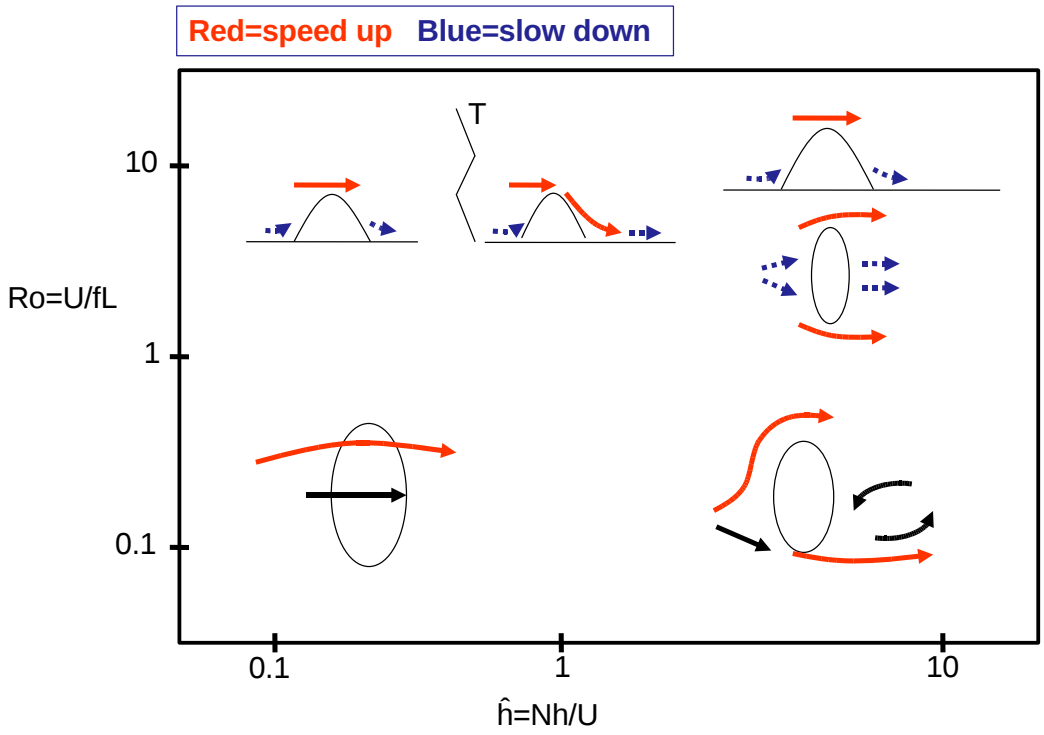

Figure 3.5: *Schematic diagram showing the combined effects of Rossby number (vertical axis) and the inverse Froude number (horizontal axis). Adapted and redrawn from Ólafsson (2003).*

of the mountain. There is, on the other hand, speed-up at the edges of the mountain. These speed-ups are sometimes referred to as corner winds or tip jets. Such a wind inbetween two mountains is called a gap wind. At high Nh/U, there may be substantial areas with hardly any wind inside the blocking and the wake, while the edges of the mountain may experience more than twofold the upstream flow speed. An intermediate flow pattern exists at values of the Nh/U close to unity (typically $0.5 < Nh/U < 3$). Here, vertically propagating gravity waves dominate the flow field. Aloft, the flow oscillates and on its way down, the flow accelerates, giving maximum surface wind speed above the slope, at the downstream foothills of the mountain. Particular structures of the flow, such as inversions or vertical variability of wind speed may enhance the wave activity, giving extreme surface winds at the bottom of the wave, downstream of the mountain.

3.2.2 Cloud microphysics

Improving quantitative precipitation forecasting (QPF) over complex topography has long been a target of research campaigns organized in the numerical weather prediction (NWP) community. Recent examples of such campaigns are the Mesoscale

Alpine Program – MAP (Bougeault et al., 2001) and the Improvement of Microphysical Parameterization through Observational Verification Experiment – IMPROVE (Stoelinga et al., 2003). Although forecasting skills of NWP models have improved considerably for many variables (e.g. geopotential height and temperature) over the past years and decades, precipitation has remained somewhat elusive (Bosart, 2003). One reason for this is that the physics governing the formation of precipitation are highly complicated, rendering parameterization difficult. Another reason is that the distribution of precipitation (particularly solid precipitation) over complex topography as simulated by NWP models is very sensitive to the dynamic and thermal characteristics of impinging wind (e.g. Chiao et al. (2004)).

According to Stensrud (2007) the reason microphycs parameterization is so challenging is twofold. Firstly, the phase changes of water that can occur in the atmosphere are numerous:

- Vapor to liquid (condensation).
- Liquid to vapor (evaporation).
- Liquid to solid (freezing).
- Solid to liquid (melting).
- Vapor to solid (deposition).
- Solid to vapor (sublimation).

As these phase changes do not occur at ideal thermodynamic equilibrium, one has both to take into account the surface tension of water drops and the surface free energy for solid particles (Stensrud, 2007). Secondly, the type of precipitation (liquid vs. solid) is strongly dependent on temperature, and as such, altitude. If the temperature is below 0°C precipitation is in general solid (exception is supercooled water). Solid precipitation can take many forms, ice crystals, snow flakes, hail, graupel, all of which vary in shape and size (different shapes and sizes are called "habits"). Furthermore, the growth of ice crystal habits is both dependent on temperature and the excess vapor density over ice. Even liquid raindrops are not homogeneous in size of shape, drops tend to grow as they fall through the atmosphere and collide with other drops that are in the way. There is however a limit to how big individual raindrops can get, and large drops have the tendency to split up when they collide with other drops.

But how does precipitation begin, how does a liquid droplet[6] form in terms of thermodynamical principles? To answer this we need to look at a modified version

[6]The distinction between a droplet and drop is usually such that the droplet is assumed to have sufficiently small terminal fall velocity that it is advected with the ambient flow. Raindrop, on the other hand, has a significant fall speed $v(R)$, where R is the radius of the drop (Cotton et al., 2011).

of the Clausius-Clapeyron equation, describing the equilibrium state for a system of water vapor over curved surface, such as a rain droplet (Stensrud, 2007) [eq. 7.1]:

$$e_s(r) = e_s(\infty)e^{2\sigma/rR_v\rho_w T} \tag{3.1}$$

Here, e_s is the equilibrium vapor pressure, σ is the surface tension, r is the radius of the droplet, R_v is the gas constant for water vapor, ρ_w is the density of water and T is temperature. Finally, $e_s(\infty)$ is the saturation vapor pressure over flat liquid surface given by the unmodified Clausius-Clapeyron equation. Equation 3.1 is often rearranged to give the saturation ratio S:

$$S = \frac{e_s(r)}{e_s(\infty)} = e^{2\sigma/rR_v\rho_w T} \tag{3.2}$$

Note that the value of S increases as r (the radius of the droplet) is reduced. A saturation ratio of 1 indicates a 100% relative humidity and that the atmosphere is just saturated. Observed ratios are typically less than 1.01, i.e. less than 1% supersaturation (Stensrud, 2007). Observations show that the first droplets to form are small ones and that the observed size of r for these droplets result in a saturation value around, or over 2, indicating a 100% supersaturation. As said before, supersaturation in the nature seldom exceeds 1%, so it is clear that droplet formation from clear water is rear.

Aerosols are microscopic particles that are present in the atmosphere. When mixed with water vapor they act to reduce the evaporation pressure and as such speed up the formation of droplets. The aerosols act as centers for condensation and are therefor called "cloud condensation nuclei" (or CCN). The size and volume of CCN's varies greatly in the atmosphere, both as a function of height, temperature and underlying surface. CCN's in a maritime air mass are bigger than CCN's in a continental air mass. This size difference leads to continental air masses having more numerous, and smaller, droplets than maritime air. Thus, in general, the collision and coalescence process is inhibited in nuclei-rich continental air. The fundamental assumption of many microphysics schemes is that the cloud droplet concentration, or activated CCN concentration, at cloud base, determine whether or not a cloud will precipitate (Cotton et al., 2011).

The presence of CCN's lead to further refinement of the saturation ratio equation for a diluted solution (Stensrud, 2007) [eq. 7.3]:

$$S = \frac{e_s(r)}{e_s(\infty)} = \left(1 - \frac{b}{r^3}\right) e^{2\sigma/rR_v\rho_w T} \tag{3.3}$$

Here, the parameter b is a function of the solute mass and density, the molecular weight of the solute and water as well as the degree of ionic dissociation[7] of the

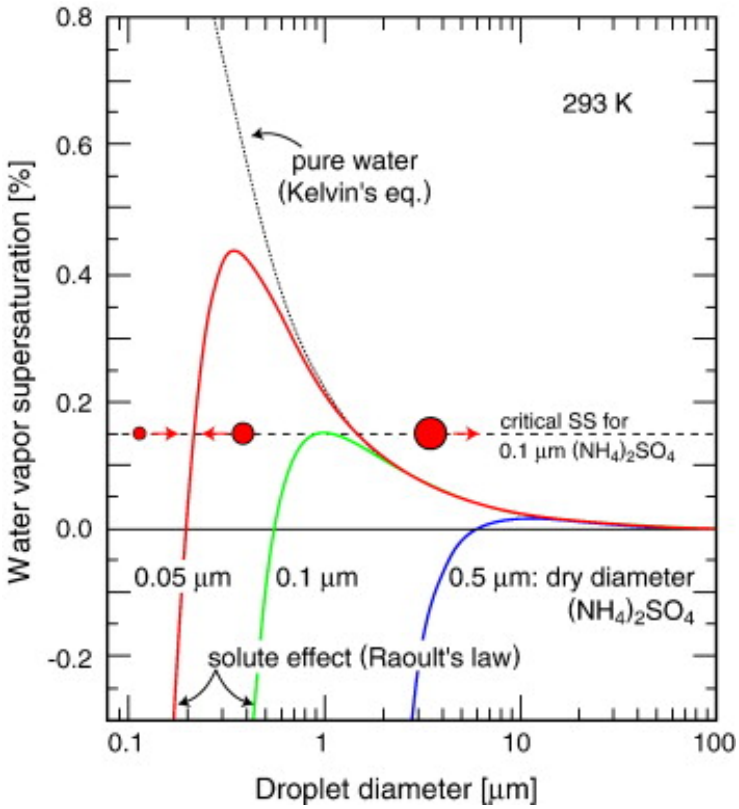

Figure 3.6: *Köhler curves showing the equilibrium water vapor supersaturation at 293 K for droplets of pure water (dotted curve) and for droplets containing various masses of dissolved $(NH_4)_2SO_4$ (solid curves) vs. diameter of the droplet. The water vapor supersaturation, $S(\%) = \left(\frac{e_s}{e_s(\infty)} - 1\right) 100$, where e_s is the partial pressure of the water vapor and $e_s(\infty)$ is the saturated vapor pressure over a plane surface of water at this temperature. In the indicated example, an ambient water vapor S of 0.15% (dashed line) exceeds the critical value for all ammonium sulfate aerosols with dry diameter $\geq 0.1\mu m$. These aerosols will therefore activate and grow into cloud droplets, whereas smaller aerosols remain as unactivated haze particles. Droplets below their corresponding equilibrium curve will shrink by evaporation whereas those above will grow by condensation (the indicated droplets correspond, for example, to a dry diameter of 0.05 µm). From Andreae and Rosenfeld (2008), reprinted with permission from Elsevier.*

solute. Figure 3.6 shows the radius r as a function of the saturation ration S at a fixed temperature, solute type and mass. The shape of r is called a Köhler-curve, it shows

[7]Dissociation is a general process in which ionic compounds (complexes, or salts) separate or split into smaller particles, ions, or radicals, usually in a reversible manner. The dissociation degree is the fraction of original solute molecules that have dissociated. From Wikipedia: http://en.wikipedia.org/wiki/Dissociation_(chemistry), retrieved on 2012-06-15.

that for a small radii the solution effect dominate and for large radii the surface tension effect dominates. Initially, the growth of the droplet is due to condensation and is proportional to $(S-1)/r$ (Stensrud, 2007). Consequently, as the droplet increases in size, its growth becomes slower and droplet growth from collisions and coalescence becomes the driving factor in transforming a droplet to a raindrop.

Freezing of cloud droplets does not necessarily happen immediately as the temperature drops below 0°C. This is because water droplets are able to maintain supersaturation relative to ice (remain as liquid water droplets and not freeze) because of the high surface tension of each micro droplet, which prevents them from expanding to form larger ice crystals (Rogers and Yau, 1989). Without ice nuclei supercooled liquid water droplets can exist down to about -40°C. If the ambient temperature is higher than -40°C, the formation of ice requires ice nuclei (IN), just as the formation of liquid droplets requires the presence of CCN.

According to Stensrud (2007) there are four processes that are believed to lead to ice nucleation. These are vapor-deposition, condensation-freezing, immersion-freezing, and contact-freezing nucleation. Contact-freezing happens when a supercooled droplet comes to a contact with an ice nucleus and freezes. Immersion-freezing is the freezing of a supercooled droplet that has an ice nuclei immersed within itself. Condensation-freezing is the condensation of water onto an ice nuclei to form a embryonic drop, followed by freezing of the embryonic drop. Once ice crystals have formed they can grow by vapor-deposition, as long as the environment is supersaturated with respect to ice. Saturation pressure with respect to water is higher than with respect to ice, this means that a cloud that is saturated with respect to water, is supersaturated with respect to ice. As ice crystals grow by vapor-deposition, the cloud can become sub saturated with respect to water but still be supersaturated with respect to ice. When this happens, water droplet start to evaporate, hence enhancing ice crystal growth. This process is called Bergeron-Findeisen mechanism of ice crystal growth (Stensrud, 2007).

As with liquid drops, collisions and coalescence can also lead to ice crystal growth. This process is called aggregation and is more complicated than for liquid phase. This is because ice crystals can come in many different forms, or habits, which affects how they interlock after collision. For liquid drops, the coalescence efficiency is near unity, but this is not the case for ice crystals. Snowflakes are formed via this process.

The process when ice crystals collide with droplet of supercooled cloud water is called riming. As the initial ice crystal collects more and more supercooled water it is gradually transformed into a particle called graupel. Although graupel density varies across a large range it is considerably greater than that of ice crystals and snowflakes. Graupel particles have typical fall speeds of 1-3 ms^{-1}, they also serve as embryos for hailstones, which have much greater fall speeds (10-50 ms^{-1}). Initiation of riming can take a long time as the original particles have very small

fall speeds as they are light and often flat in shape. But once the particles begin to fall, riming can be very effective in growing the ice crystals into graupel particles, assuming there is sufficient supercooled cloud water.

3.3 Modeling of surface winds and precipitation

Atmospheric models are systems of differential equations derived from the basic laws of physics, fluid motion, and chemistry. These are the momentum equations that represent Newtons second law of motion[8], and the thermodynamic equation that accounts for both diabatic and adiabatic changes in temperature. In addition there are the continuity equations for total mass and water vapor and the gas law, that relates temperature, pressure and density. These equations were first described in Bjerknes's 1904 paper *Das Problem der Wettervorhersage, betrachtet vom Standpunkte der Mechanik und der Physik*. The details of the equations where set out by Lewis Fry Richardson and published in his book *Weather prediction by numerical process* in 1922. Following Warner (2011) we now write these equations in their primitive form for a spherical earth:

$$\frac{\partial U}{\partial t} = -U\frac{\partial U}{\partial x} - V\frac{\partial U}{\partial y} - W\frac{\partial U}{\partial z} + \frac{UV\tan\phi}{a} - \frac{UW}{a} - \frac{1}{\rho}\frac{\partial p}{\partial x} - 2\Omega(W\cos\phi - v\sin\phi) + \mathbf{Fr_x} \tag{3.4}$$

$$\frac{\partial V}{\partial t} = -U\frac{\partial V}{\partial x} - V\frac{\partial V}{\partial y} - W\frac{\partial V}{\partial z} + \frac{U^2\tan\phi}{a} - \frac{UW}{a} - \frac{1}{\rho}\frac{\partial p}{\partial y} - 2\Omega U\sin\phi + \mathbf{Fr_y} \tag{3.5}$$

$$\frac{\partial W}{\partial t} = -U\frac{\partial W}{\partial x} - V\frac{\partial W}{\partial y} - W\frac{\partial W}{\partial z} - \frac{U^2+V^2}{a} - \frac{1}{\rho}\frac{\partial p}{\partial z} + 2\Omega U\cos\phi - g + \mathbf{Fr_z} \tag{3.6}$$

$$\frac{\partial T}{\partial t} = -U\frac{\partial T}{\partial x} - V\frac{\partial T}{\partial y} + (\lambda - \lambda_d)W + \frac{1}{c_p}\frac{\mathbf{dH}}{\mathbf{dt}} \tag{3.7}$$

$$\frac{\partial \rho}{\partial t} = -U\frac{\partial \rho}{\partial x} - V\frac{\partial \rho}{\partial y} - W\frac{\partial \rho}{\partial z} - \rho\left(\frac{\partial U}{\partial x} + \frac{\partial V}{\partial y} + \frac{\partial W}{\partial z}\right) \tag{3.8}$$

$$\frac{\partial q_v}{\partial t} = -U\frac{\partial q_v}{\partial x} - V\frac{\partial q_v}{\partial y} - W\frac{\partial q_v}{\partial z} + \mathbf{Q_v} \tag{3.9}$$

$$p = \rho RT \tag{3.10}$$

[8]Newton's second law of motion states that the net force on a particle is equal to the time rate of change of its linear momentum $\mathbf{p}$ in an inertial reference frame: $F = \frac{d\mathbf{p}}{dt} = m\frac{d\mathbf{v}}{dt}$, where m is mass, and $\mathbf{v}$ is speed (Feynman et al., 1963)

where U, V, and W represent the three dimensional winds, ρ is the density of air, p is pressure, T is temperature. Ω is the rotational frequency of earth, ϕ is latitude, λ is the lapse rate and λ_d is the dry adiabatic lapse rate, c_p is the specific heat at constant pressure, g is gravitational acceleration, and R is the gas constant for ideal gas. Here, Fr represents frictional terms, and H and Q_v represent sources and/or sinks of heat and humidity, respectively. These terms, which are written in bold, need to be parameterized within the model.

These equations cannot be solved analytically but have to be converted to a form that can be solved by numerical methods on fast computers. Traditionally this is done by a method called Reynolds averaging, where a variable is split into a *mean* (defined as a mean value over a grid cell) and *turbulent* part. The time development of the mean part of a variable can be directly resolved by the model (often referred to as the *dynamical core* of the model) but the turbulent part represents unresolved effects. These effects need to be described, or parameterized, in terms of resolved parts of the equations. Methods to do so will be described in section 3.3.1.

In addition to Reynolds averaging, the equations need to be formulated on a grid of some sort. There are a number of methods to do so, but the two most common are the method of finite differences (also known as the grid-point method) and the spectral method. The spectral method dominates global modeling as it levitates singularities at the poles that early global models, using finites differences, were riddled with. This is done be replacing the finite expansions of the variables with Fourier series, or Fourie-Legendre functions, to represent the horizontal spatial variation. In the finite difference method a procedure is defined for organizing grid points in a systematic way over the area of interest, the grid needs not even be regular (Warner, 2011).

In order to solve the equations the whole planet, or a sub-region of interest, is covered by a 3-dimensional grid to which the basic equations are applied and evaluated. At each grid point the motion of the air (winds), heat transfer (thermodynamics), radiation (solar and terrestrial), moisture content (relative humidity) and surface hydrology (precipitation, evaporation, snow melt and runoff) are calculated as well as the interactions of these processes among neighboring points (cf. Fig. 3.7). The computations are stepped forward in time from days to seasons, or even to centuries depending on the study. State-of-the-art coupled ocean-atmosphere models now include interactive representations of the ocean, the atmosphere, the land, hydrologic and cryospheric processes, terrestrial and oceanic carbon cycles, and atmospheric chemistry. The accuracy of these models is limited by lack of observations, grid resolution and our ability to describe the complicated atmospheric, oceanic, and chemical processes mathematically. Despite some imperfections, models simulate remarkably well current climate and its variability (IPCC, 2007). More capable supercomputers enable significant model improvements by allowing for more accurate representation of currently unresolved physics.

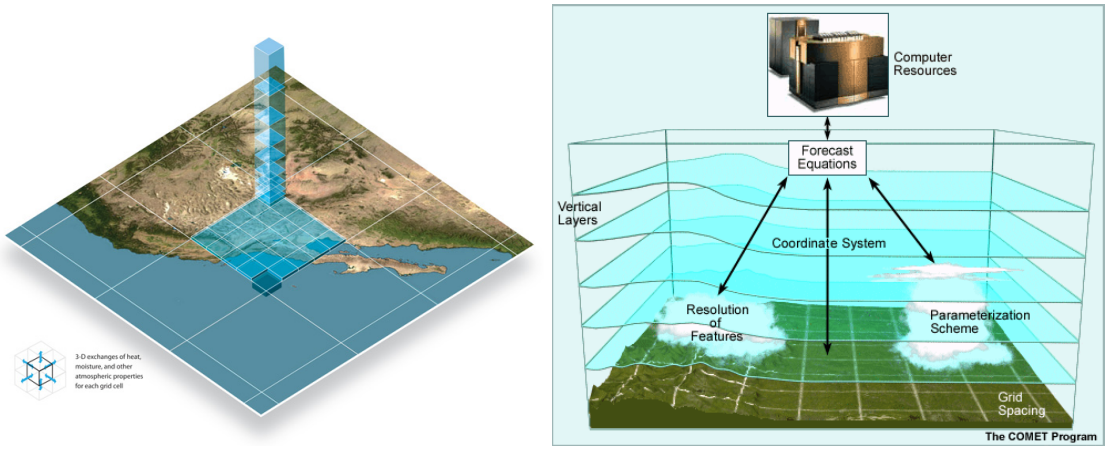

Figure 3.7: *Atmospheric models are systems of differential equations based on the basic laws of physics. The models calculate winds, heat transfer, radiation, relative humidity, and surface hydrology within each grid box and evaluate interactions with neighboring points. Figure courtesy of UCAR*[9].

As of autumn 2012, the horizontal grid resolution of the two most widely used global atmospheric forecast models is about 14 and 28 km (0.125°and 0.25°). These models are the European Centre for Medium range Weather Forecasts – ECMWF model, and the Global Forecast System – GFS model, respectively. Both modeling system simulate weather forecasts four times a day for the whole globe that span over two weeks.

Even at such high horizontal resolution, many important flow features are left unresolved. To tackle this shortcoming of the global models, one can use regional, or local area, weather models. These models only cover a fraction of the globe (hence the name regional, or local area) and are typically forced by initial and boundary data from a global model. Consequently they can be run at a higher horizontal resolution for the fraction of the computation power that would otherwise have been needed to run the global models at the same resolution. As the true orography is better resolved, so to the interaction between the surface and the atmospheric flow can be better resolved. These improvements in the simulated flow can be expected to be especially evident in mountainous regions like Iceland.

But how are winds and precipitation simulated within an atmospheric model, global or regional? An important feature of any numerical atmospheric model are the parameterization schemes. It is within these schemes, and through their interaction, that the various processes within the atmosphere are simulated. We will now look in more detail on two types of parameterization schemes that are of great importance when simulating surface winds and precipitation. These are the planetary

[9]http://www2.ucar.edu/news/understanding-climate-change-multimedia-gallery, left figure, and http://www.meted.ucar.edu/mesoprim/models/print.htm, right figure. Retrieved on 2012-06-23.

boundary layer schemes and the microphysics schemes.

3.3.1 Planetary boundary layer schemes

The lowest part of the atmosphere is generally called the atmospheric boundary layer, the planetary boundary layer, or simply the boundary layer. The depth, or thickness, of the boundary layer is typically defined as the distance through which energy fluxes from the earth's surface (e.g. temperature change or a forced ascend due to an obstacle) can reach within one hour. Stull (1988) [p. 2] defines the boundary layer as "the part of the troposphere that is directly influenced by the presence of the earth's surface, and responds to surface forcings with a timescale of an hour or less[10]". It is within this part of the atmosphere that we humans spend the bulk of our live.

The depth of the boundary layer typically varies between 1 and 2 km, but can range from tens of meters to 4 km or more (Stull, 2006) [p. 375]. In atmospheric modeling the generation of these surface energy fluxes are parameterized using different models from the PBL models. These Land Surface Models (LSM) handle the interaction between the earths surface (both land and water) and the atmosphere as well as modeling the interaction between soil and vegetation and the atmosphere. It is through the LSM's that the surface energy fluxes are described and in turn form a lower boundary condition for the PBL models. How these energy fluxes influence the lower atmosphere depends on the PBL scheme.

The transport of energy up through, and within, the boundary layer is turbulent in nature. The source of turbulence can both be sensible heat flux from the ground (warm air being more buoyant than cold) and wind shear. The relevant importance of these two main sources of turbulence varies both temporarily (e.g. more heat flux during the daytime than at night) and spatially.

The equations of motion could in theory be applied directly to turbulent flow. This would however require very small grid spacing in order for the model to correctly simulate the flow behavior. Even with a grid spacing of 50 meters, there would still be sub-grid eddies whose influence on the flow would need to be accounted for. A common method to describe the effects of sub-grid eddies in contributing to the overall mixing in the boundary layer is called Reynolds averaging. Reynolds averaging gives a statistical approach to the eddy effects. The idea behind the technique is to separate a variable into a time averaged part and a perturbing part.

$$U = \bar{u} + u' \tag{3.11}$$

[10] It should be noted that this only applies to fluxes of moisture, heat and momentum. Perturbations due to surface-generated gravity waves are obviously outside the framework of this definition, as such waves may travel fast through the entire troposphere and further upwards

The $\bar{u}$ can also be regarded as the part of U that can be resolved on the grid of the numerical model in question. Consequently, the perturbation part, the $\overline{u'}$, is the sub-grid fluctuation around the grid-resolved value. The perturbations are defined such that their time average equals zero (i.e. $\overline{u'} = 0$). Also, the product of two variables, U, and V, give:

$$UV = \overline{u}\overline{v} + \overline{u'v'} \tag{3.12}$$

When using this technique on the momentum equations, the perturbations are assumed to represent the effects of turbulence. For a detailed description of how this is done, we refer to Stull (1988) and Stensrud (2007). Following Stensrud (2007) we define the following:

- x_j as a generic distance, with $x_1 = x, x_2 = y, x_3 = z$
- u_j as a vector, with $u_1 = u, u_2 = v, u_3 = w$
- δ_j as a unit vector, with $\delta_1 = i, \delta_2 = j, \delta_3 = k$

and δ_{mn} as the Kronecker delta which equals 1 when $m = n$ but is zero otherwise. Finally, we define the unit tensor ε_{ijk} as:

$$\varepsilon_{ijk} = \begin{cases} +1, & \text{if } i,j,k \text{ are in ascending order} \\ -1, & \text{if } i,j,k \text{ are in descending order} \\ 0, & \text{otherwise} \end{cases}$$

using this, the equations of motions, assuming the Boussinesq assumption and after Reynolds averaging, can be written like this (eq. 5.12 in Stensrud (2007)):

$$\frac{\partial \bar{u}_i}{\partial t} + \bar{u}_j \frac{\partial \bar{u}_j}{\partial x_j} = -\delta_{i3} g + f \varepsilon_{ij3} \bar{u}_j - \frac{1}{\bar{\rho}} \frac{\partial \bar{p}}{\partial x_i} + \nu \frac{\partial^2 \bar{u}_i}{\partial x_j^2} - \frac{\partial \overline{(u_i' u_j')}}{\partial x_j} \tag{3.13}$$

The second term on the right hand side represents the Coriolis effect and the fourth term represents molecular viscosity, and is generally ignored in praxis. The last term on the right hand side is the covariance, or Reynolds stress, term. As this term is not predicted explicitly it can either be parameterized, or additional equations can be derived to predict it. Doing the latter will however result in yet more terms that are not explicitly predicted (namely $\partial \overline{u_i' u_j' u_k'} / \partial x_j$). The unknown is now a triple correlation term. If one would derive equations to solve for these, one would in turn create a quadruple term, and so on, and so on. This cascade of creation of unknown terms is referred to as the *turbulence closure* problem.

As there will always be more unknowns than there will be equations one needs, at some point, to parameterize the solution for the unknown terms by relating them

in some way to known variables. It is these unknown terms that contain the unresolved sub-grid motion. It is through the closure formulation (or parameterization) that the mixing from the sub-grid is introduced into the equations for large scale motions (the resolved part of the motion) within the PBL scheme. It is important to note that this sub-grid mixing, as handled by PBL schemes, is one-dimensional. That is, mixing in the horizontal is assumed to be an order, or orders, of magnitude less than in the vertical. Hence, its effects are dismissed when the equations of motion are derived for the various PBL schemes. This assumption breaks down when the horizontal scale of the model becomes of the same order of magnitude as the length scale of the energy- and flux-containing turbulence. This numerical region is termed "Terra Incognita" by Wyngaard (2004).

The "order" (also called "level") of a PBL scheme refers to where in this cascade of terms one decides to parameterize the correlation terms. First order schemes only include equations for the state variables (u, v, w, T, q), i.e. winds, temperature and humidity (also known as first moments). The covariance terms, like $\overline{u'v'}$, are parameterized. Second order schemes in turn include explicit description of both the first moments and the covariance terms, but parameterize the triple correlations terms. There are also PBL schemes were not all of the covariance terms are explicitly described, such schemes are referred to as 1.5-order schemes. The main reason for using higher order is the assumption that crude description of the third moments (i.e. parameterization of the triple correlation terms) will give a better forecast of the second moments.

Another deciding factor for a PBL scheme is how the equations are integrated vertically. If only neighboring points are used, the scheme is referred to as being "local" (or "local closure" scheme). On the other hand, if information from the whole vertical column is used, the scheme is called "non-local" (also known as "non-local closure" schemes). Local and non-local PBL schemes both have their pros and cons. In general, non-local scheme are better equipped to describe dry convective boundary layers that typically evolve over warm areas such as summertime Arizona. Under such conditions the day-time boundary layer can become very deep. Bright and Mullen (2002) report of 2 km deep boundary layer, and even exceeding 3 km depth. In this study, Bright and Mullen (2002) also showed that local PBL schemes consistently under predicted the depth of the day-time Arizona boundary layer, often by a factor of two. The local schemes also over predicted the convective available potential energy (CAPE) by a factor of two, whilst non-local schemes performed well under these conditions. The reason local closure scheme have difficulties under these conditions is that the vertical mixing is to a large extent governed by very large eddies. Hence, relative difference in the vertical transport between few model levels is negligible. In short, the local models don't see the "big picture". A clear benefit local closure models of order 1.5, or higher, do have over non-local ones is the ability to predict the intensity of turbulent kinetic energy

(TKE). Information about TKE is important for air quality studies and dispersion studies in general, e.g. to model the distribution of volcanic ash in the atmosphere.

The dominant mechanism for boundary layer development is turbulence. During daytime production of turbulence is in general dominated by buoyancy gradients produced by surface forcing. Wind shear is usually the dominant factor in turbulence production at night. As horizontal resolution is increased horizontal gradients of wind shear may contribute to the production of turbulence. At present, only vertical movement is taken into consideration, the PBL schemes are one dimensional. Direct influences of clouds on the development of the boundary layer are not included either.

Closure constants for PBL schemes are in general estimated from observed data. This data in turn stems from relatively few observations periods and/or locations. Generally, the data is collected in areas where the terrain is flat and the land use characteristics is homogeneous. This is done in order to observe the boundary layer development under pristine conditions. This may however result in the development of BL schemes that have considerable problems simulating the development of arctic boundary layer or the boundary layer in complex terrain.

3.3.2 Microphysics schemes

Warner (2011) lists up a number of microphysical processes that need to be parameterized in a numerical model:

- Condensation – Liquid droplets form when water saturation is exceeded at temperature from -40°C to above freezing. The condensation takes place on CCN particles.

- Accretion – In the warm-cloud process, i.e. within clouds that the ice phase does not play a significant role, droplets with different masses have different fall velocities, and the resulting collisions between droplets can result in coalescence and droplet growth. As a droplet grows, so does its vertical velocity relative to smaller droplets, thus increasing the rate of collisions.

- Accretion by frozen particles – Snow, graupel, or hail collect other solid or liquid particles as they fall.

- Evaporation – Cloud droplets and raindrops can evaporate.

- Ice and snow aggregation – Aggregation is the process when ice crystals and snow flakes collide and coalesce.

- Vapor deposition – Ice crystal growth via the Bergeron-Findeisen mechanism.

- Melting – As snow flakes fall into the lower troposphere, below the freezing level, they may melt and form raindrops. Similarly, hail and graupel begin to melt as they fall below freezing level.
- Freezing – Water droplets freeze in the presence of IN, riming involves the freezing of water droplets that collide with ice crystals, and raindrops can freeze to form graupel.

Microphysical schemes are typically grouped into "bulk" and "bin" models. Bulk models use a distribution function (e.g. that of Marshall and Palmer (1948)) to describe the distribution of hydrometeors in the atmosphere. These models predict the particle mixing ratio (total mass per unit volume of air), and sometimes the total particle concentration as well. The former are named single-moment schemes, and the latter double moment schemes. The benefit of using double-moment compared to single-moment methods is that they predict both number concentration and mixing ratio and are therefore able to derive the broad features of the drop size distribution. In doing so, the double-moment scheme improves the representation of growth processes and precipitation formation (Cotton et al., 2011) and as such can be used over a wider range of environments. Triple-moment scheme also exist, but only if the distribution is described using a Gamma[11] function. In that case, the third moment describes the shape parameter k (Warner, 2011). In contrast, bin models do not use distribution functions but instead divide the particle distribution into a finite number of categories (or "bins"). The particle distribution into bins requires considerable more computing power than the bulk approach and a poor knowledge on ice phase physics results in potentially inaccurate representation of the evolution of ice particle concentrations (Stensrud, 2007). Due to this, bin models are currently not part of any operational models, unlike bulk schemes, and are used only in a few research models.

3.3.2.1 Bin parameterizations

The approach to model microphysics processes in clouds by explicitly resolving the evolution of hydrometeor size spectra is referred to as the bin-resolving technique. The temporal evolution of the spectral density $f(m)$ of cloud droplets of mass m to $m \pm \delta m/2$ can be written as (Cotton et al., 2011):

$$\begin{aligned}\frac{\partial f(m)}{\partial t} =& N(m) - \frac{\partial[\dot{m} f(m)]}{\partial m} + G(m)|_{\text{gain}} + G(m)|_{\text{loss}} \\ &+ B(m)|_{\text{gain}} + B(m)|_{\text{loss}} + \tau(m)\end{aligned} \tag{3.14}$$

[11] In probability theory and statistics, the gamma distribution is a two-parameter family of continuous probability distributions. It is common to parameterize it with a shape parameter k and a scale parameter θ. From Wikipedia: http://en.wikipedia.org/wiki/Gamma_distribution, retrieved on 2012-06-18.

where $\dot{m}$ is the total derivative of the mass, $\dot{m} = \frac{Dm}{Dt} = \frac{\partial m}{\partial t} + u\frac{\partial m}{\partial x} + v\frac{\partial m}{\partial y} + w\frac{\partial m}{\partial z}$.

In (3.14) N represents nucleation, G represents collection, B represents breakup, and τ represents the sum of both mean and turbulent transport processes. N is the production of droplets of mass m by the nucleation of such droplets on activated CCN. This term is kept in (3.14) only if the droplet spectrum $f(m)$ is truncated at some small droplet mass. The second term on the right hand side is the divergence of $f(x)$ due to continuous vapor mass deposition on droplets growing at a rate of $\dot{m}$, where $\dot{m}$ is a function of the droplet mass, its solubility in water, and the local cloud supersaturation. The third and fourth terms represent, respectively, the gain and loss due to the collision and coalescence of cloud droplets. The fifth and sixth terms represent, respectively, the gain and loss of the spectral density $f(m)$ due to breakup of droplets.

A common approach to solve (3.14) is to discretize $f(m)$ into 40 to 70 elements and then integrate the equations by finite element approach (Cotton et al., 2011).

3.3.2.2 Bulk parameterizations

The distribution of ice and liquid particles in the atmosphere can, to a certain extent, be described by an inverse exponential function, first suggested by Marshall and Palmer (1948):

$$n(D) = n_0 e^{-\lambda D} \tag{3.15}$$

where D is the particle diameter (m), n is the number of particles per unit volume (m^{-4}), λ is the slope parameter that defines the fall off of particles as the diameter increases (m^{-1}), and n_0 is the intercept parameter that defines the maximum number of particles per unit volume at $D = 0$ size (Stensrud, 2007). The gamma distribution has also been used to describe particle distribution, it differs from that of Marshall and Palmer mainly for very small droplets.

An important assumption that is generally made within bulk models is that non-precipitating hydrometeors have zero fall speed, i.e. they simply move with the ambient flow. It is not until the droplet (liquid or solid) has reached a certain size that it can be regarded as a precipitating particle (raindrop, snowflake, hail, or graupel particle). Berry and Reinhardt (1974) demonstrated that a natural break between cloud and raindrops occurs at a radius of 50 μm.

The bulk microphysics schemes differ greatly in complexity, both with regard to how many types of interactions between particles are assumed (phase and habit changes) and also how the interactions between different particles are described. The equations that describe the evolution of the microphysical variables do however

all follow a similar structure:

$$\frac{\partial q_x}{\partial t} = -ADV(q_x) + TURB(q_x) + (P_1 + P_2 + P_3 + P_4 + P_5 + \cdots) \tag{3.16}$$

where q_x is any microphysical variable (e.g. mixing ratios of water vapor, cloud water, rainwater, ice, snow, and graupel), ADV represents the advective processes, $TURB$ the turbulent processes and P_i represents the various tendencies from the microphysics parameterization (Stensrud, 2007).

Parameterization of warm rain condensation The approach to create condensed particles in microphysical parameterization schemes differs somewhat from what happens in nature and was described in section 3.2.2. Rather than predicting the aerosol composition itself (like size, shape and chemical properties), and from it predict the droplets formation and growth the scheme rather try to forecast the droplet formation based on other known model parameters, in particular the mixing ratios. To predict aerosol development and resulting droplet formation would be a fiendishly complex task.

Following Stensrud (2007) we now describe how the increase in cloud water, due to condensation, over a single integration time step is approximated. The methodology follows that of Asai (1965) and is used in most bulk microphysics schemes.

When water vapor condenses and cloud droplets are formed the following supersaturation conditions is assumed to hold:

$$q_v - q_{vs} = \delta M > 0 \tag{3.17}$$

where q_v is the water vapor mixing ratio, q_{vs} is the saturation vapor mixing ratio, and δM represents the total possible condensed water. Note that δM is the sum of two variables; δM_1 is condensed water and δM_2 is the increase in the water vapor mixing ratio stored in the air. The latter variable is due to latent heat release from condensation that increase the air temperature and consequently the saturation mixing ratio. The equation for latent heat

$$\theta = T\left(\frac{p_0}{p}\right)^{R/c_p} \tag{3.18}$$

can be used to express the warming due to condensation

$$\delta\theta = \frac{L_v}{c_p}\left(\frac{p_0}{p}\right)^{R/c_p}\delta M_1 \tag{3.19}$$

where L_v is the latent heat of vaporization that is needed to be given to a unit mass of material to convert it from liquid to vapor without changing the temperature. The specific heat at constant pressure is denoted by c_p, p_0 is the surface pressure, and p is the pressure. The Clausius-Clapeyron equation for the variation of the equilibrium vapor pressure e_s with temperature T can be written as (Wallace and Hobbs, 2006):

$$\frac{de_s}{dT} = \frac{L_v}{T(\alpha_v + \alpha_l)} \tag{3.20}$$

where α_v is the unit mass of vapor and α_l is the unit mass of liquid. As $\alpha_v \gg \alpha_l$, equation (3.20) can be approximated as:

$$\frac{de_s}{dT} \simeq \frac{L_v}{T\alpha_v} \tag{3.21}$$

Because α_v is the specific volume of water vapor that is in equilibrium with liquid water at temperature T, the pressure it exerts at T is e_s. Therefore, from the ideal gas equation for water vapor, $e_s\alpha_v = RT$, we can rewrite equation (3.21) as:

$$\frac{de_s}{dT} = \frac{L_v e_s}{R_v T^2} \tag{3.22}$$

The partial pressure exerted by any constituent in a mixture of gases is proportional to the number of moles of the constituent in the mixture. Therefore, the pressure e due to water vapor in air is given by (Wallace and Hobbs, 2006):

$$e = \frac{n_v}{n_v + n_d} p = \frac{\frac{m_v}{M_w}}{\frac{m_d}{M_d} + \frac{m_v}{M_w}} p \tag{3.23}$$

Here, n_v and n_d are the number of moles of water vapor and dry air in the mixture, respectively, M_w is the molecular weight of water, M_d is the apparent molecular weight of dry air, and p is the total pressure of the moist air. As the mixing ratio q_v is defined as m_v/m_d (i.e. the ratio between the mass of water vapor to that of the mass of dry air) one can re-write equation (3.23) as:

$$e = \frac{q_v}{q_v + \varepsilon} p \tag{3.24}$$

where

$$\varepsilon = \frac{R_d}{R_v} = \frac{M_w}{M_d} = 0.622$$

where R_d and R_v are the individual gas constants for dry air and water vapor, respectively. As $\varepsilon \gg q_v$ equation (3.24) can be simplified to:

$$e \simeq \frac{q_v p}{\varepsilon} \tag{3.25}$$

We can now use equation (3.25) to rewrite equation (3.22) as:

$$d\left(\frac{q_{vs}p}{\varepsilon}\right) = \frac{L_v(q_{vs}p/\varepsilon)}{R_v T^2} dT$$

which, at a constant pressure, simplifies to

$$dq_{vs} = \frac{L_v q_{vs}}{R_v T^2} dT \tag{3.26}$$

We now use the equation for potential temperature (3.18) to replace dT for $d\theta$ in equation (3.26), such that

$$dq_{vs} = \frac{L_v q_{vs}}{R_v \theta^2} \left(\frac{p_0}{p}\right)^{\kappa} d\theta \tag{3.27}$$

where $\kappa = R/c_p$. Finally, replace $d\theta$ with $\delta\theta_1$ to represent the warming effect of condensation and dq_{vs} with δM_2 to represent the increased saturation mixing ratio due to warming. This leads to (Stensrud, 2007)

$$\delta M_2 = \frac{L_v^2}{c_p R_v} \left(\frac{p_0}{p}\right)^{2\kappa} \frac{q_{vs}}{\theta^2} \delta M_1 \tag{3.28}$$

and so the ratio of $\delta M_1/\delta M$ is

$$\frac{\delta M_1}{\delta M} = r_1 = \frac{1}{[1 + (L_v^2/c_p R_v)(p_0/p)^{2\kappa}(q_{vs}/\theta^2)]} \tag{3.29}$$

The increase in cloud water over a single model time step Δt due to condensation, P_{COND}, is

$$P_{COND} = (r_1 \delta M)/\Delta t \tag{3.30}$$

The value of P_{COND} is the number of droplets created by condensation over the integration time step Δt. In some microphysics schemes, the value of the adjustment factor r_1 is held constant, but in general it varies between values of 0.25 to 0.9 for a lapse rate of 6.5°C/km^{-1} (Asai, 1965). If the supersaturation of the environment is less than a chosen critical value, evaporation occurs using the same parameterization. In theory this value should be 1, i.e. 100% Relative Humidity, but in reality it often needs to be less in order for the scheme to be able to start producing droplets via condensation. The reason is that it may be very difficult for a scheme to make a whole grid box supersaturated, especially if the model resolution is relatively coarse. Currently, for the GFS global model (which has a horizontal resolution of $0.25^\circ \simeq 28$km) this critical value is set to 0.85, i.e. at 85% Relative Humidity, the scheme starts producing droplets via warm rain condensation.

Parameterization of ice initiation The representation of ice-phase microphysical processes in a cloud model is greatly complicated by the variety of forms of the ice phase, as well as by the numerous physical processes that determine the crystal forms. Moreover, in contrast to the physics of warm rain formation, the physics of ice-phase is less understood. The result is that in many cases the formulation of parameterization schemes for ice-physics, based on detailed theoretical models and/or observations, cannot be done (Cotton et al., 2011).

Stensrud (2007) states that observed concentrations of ice nuclei appears to be sufficient to explain ice crystal concentration in some atmospheric clouds. Knowing the ice nuclei concentrations makes it possible to calculate the concentration of vapor-activated ice crystals. Given the ice crystal concentration, knowledge of the mass of a typical ice crystal is sufficient to calculate the value for the cloud ice mixing ratio. Consequently, most parameterization schemes assume that cloud ice forms when in the presence of ice nuclei when the air is supersaturated with respect to ice and the air temperature is below freezing. This assumption allows observations of ice nuclei to be used as the basis for these schemes.

Fletcher (1965) derived an empirical formulation relating the formation of ice nuclei with temperature:

$$N_{IN} = A\exp(\beta T_s) \tag{3.31}$$

where N is the number concentration of active ice nuclei per liter of air, T_s is the number of supercooling (the temperature in °C), β varies from about 0.3 to 0.8 and A is about 10^{-5} liter^{-1} (Cotton et al., 2011). The initiation rate of cloud ice is then described as (Stensrud, 2007):

$$P_{ICE} = \left(\frac{m_i n_c}{\rho} - q_i\right)\frac{1}{\Delta t} \tag{3.32}$$

where q_i is the cloud ice mixing ratio, m_i is the mass of a typical ice particle and Δt is the integration time step of the model. A different relationship between ice particle number concentration and temperature is proposed in Meyers et al. (1992):

$$n_c = 1000\exp\left[-0.639 + 12.96\left(\frac{q_v}{q_{vsi}} - 1\right)\right] \tag{3.33}$$

where q_{vsi} is the saturation water vapor mixing ratio over ice. Dudhia (1989) uses the Fletcher parameterization for ice initiation but Reisner et al. (1998) indicate that the Fletcher scheme overestimates ice nucleation at very low temperatures. Consequently, the value of T is not allowed to go below a certain threshold value ($T = 246$K) in the Reisner scheme. Equation (3.33) is used in the scheme of Schultz (1995), but is not allowed if ice is already present. This is done because ice nucleation is a much slower process than deposition growth of ice crystals (Stensrud, 2007).

The simple Dudhia (1989) scheme regards solid hydrometeors either as snow or ice if the temperature is less than 273 K, with these hydrometeors turning into rain and cloud water, respectively, if the temperature rises. The interactions between the hydrometeor types are also relatively simple; ice can turn into snow and water vapor, water vapor can turn into ice or snow, but snow can only turn into vapor. If the temperature is above the freezing level of water than vapor can only turn into cloud water, cloud water can turn into vapor or rain, and rain can only turn into vapor (cf. Fig. 3.8). Other schemes can be considerably more complicated, allowing for

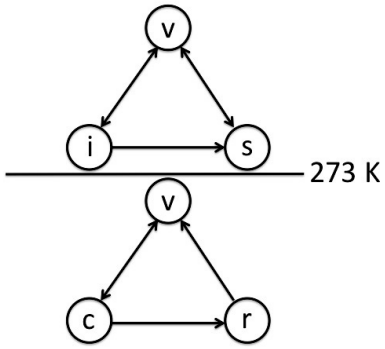

Figure 3.8: *Illustration of the michrophysical processes available in Dudhia (1989) microphysics scheme. Adapted from Stensrud (2007).*

the existence of all hydrometeors at the same time and various interactions between said hydrometeors.

As most microphysics schemes assume that non precipitating hydrometeors are advected with the ambient flow it is clear that the description of the boundary layer can greatly affect the precipitation field. It should however be noted that the description of the microphysical processes do also affect the boundary layer behavior. This can be explained by a simple thought experiment. Envision a parcel of moist air being advected towards a mountain. As the parcel approaches the obstacle it is forced to ascend and is no longer in equilibrium with its environment. Through adiabatic processes there will be a change (either positive of negative) of heat due to forced phase change of the parcel. This heat change in turn can affect the static stability of the layer, and if this layer is near the mountain height, upstream of the mountain, this can enhance, or diminish, the likelihood of a down-slope wind-storm. The importance of this mechanism was demonstrated in Rögnvaldsson et al. (2011).

3.4 Dynamical downscaling

Dynamical downscaling is a method for obtaining high resolution climate, or climate change, information from relatively coarse resolution global climate models (GCMs). Typically, GCMs have a resolution of 100-200 km by 100-200 km. Figure 3.9 shows how the resolution of global models, used for the IPCC evaluation reports, has increased over the years. Many impact-models require information at

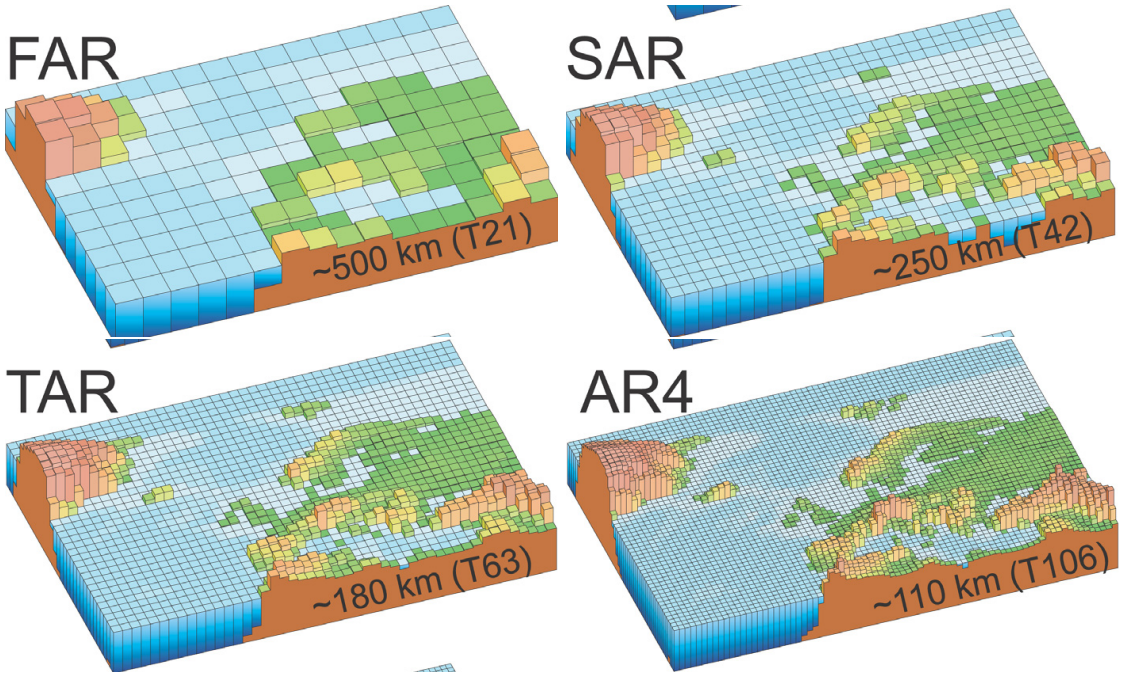

Figure 3.9: *The horizontal grid resolution of the global models used for the IPCC climate evaluation reports has steadily increased. Figure courtesy of IPCC, http://www.icpp.ch.*

scales of 10 km or less, so some method is needed to estimate the smaller-scale information.

The idea behind dynamical downscaling is relatively simple. Take output from a coarse resolution model, e.g. a Global Circulation Model (GCM), and use it to force a Limited Area Model (LAM) at a higher horizontal and vertical resolution. As resolution is increased, processes governed by the interaction of the large scale flow and topography become better resolved by the models. One drawback of this approach, which is not present in global climate models, is that the simulations are dependent on the lateral boundary conditions. These can constrain the model dynamics and hence affect the results (e.g. Warner et al. (1997)). To minimize the constraining effects of the boundary conditions, Qian et al. (2003) suggested consecutive short term integration, overlapping in time as to minimize the effects of spin-up, instead of a single long term integration. Other investigators (e.g. Giorgi

and Mearns (1999)) opt for longer integration times, emphasizing the importance of the model to be free to develop its own internal circulations.

It should be pointed out that state of the art LAM, such as the WRF model, have the possibility of “nesting”, i.e. one can create a relatively coarse outer domain and “nest” smaller domains, at a higher horizontal resolution, within this “mother of all domains” (MOAD). This approach can than be used to minimize the negative effects of coarse resolution boundary effects, granted that the MOAD is sufficiently large to allow the LAM to create its own atmospheric flow.

Chapter 4

Overview of peer reviewed articles

4.1 Paper I: Mapping of precipitation in Iceland using numerical simulations and statistical modeling

Precipitation in Iceland during a period of 10 years is simulated with the PSU/NCAR MM5 model. The results are compared with precipitation estimated by a statistical model based on observations and a number of topographic and geographic predictors. The simulated precipitation pattern agrees with the statistical model in areas where data is available and gives a credible precipitation pattern in data-sparse mountainous regions. The simulation is however in general overestimating the precipitation, but the magnitude and the seasonal and geographical distribution of the overestimation indicate that it is to some extent associated with observation errors that are due to wind-loss of solid precipitation. There are also uncertainties associated with the representativeness of the observations as well as with the reference model itself.

4.2 Paper II: Numerical simulations of precipitation in the complex terrain of Iceland – Comparison with glaciological and hydrological data

Atmospheric flow over Iceland has been simulated for the period September 1987 through June 2003, using the PSU/NCAR MM5 mesoscale model driven by initial and boundary data from the European Centre for Medium-range Weather Forecasts (ECMWF). The simulated precipitation is compared with two types of indirect precipitation observations. Firstly, snow accumulation on two large ice caps in SE-

Iceland and on two large glaciers in central Iceland. Secondly, model output is used as input to theWaSiM-ETH hydrological model to calculate and compare the runoff with observed runoff from six watersheds in Iceland for the water years 1987–2002. Model precipitation compares favourably with both types of validation data. The seasonal and inter-annual variability of precipitation is investigated at low as well as high altitudes. The simulations reveal a negative trend in the winter precipitation in W-Iceland, but a positive trend in the ratio of lowland precipitation to mountain precipitation in E-Iceland. There is in general a substantial inter-annual variability in the ratio of lowland precipitation to precipitation in the mountains, especially in E-Iceland, emphasizing the limitation of precipitation observations in the lowlands as a proxy for precipitation in the mountains. In order to assess the impact of orography on the precipitation climate of Iceland, precipitation is simulated with flat Iceland and compared to a simulation with true orography. It is found that the mountains contribute to a total increase of precipitation in Iceland of the order of 40%.

4.3 Paper III: Sensitivity simulations of orographic precipitation with MM5 and comparison with observations in Iceland during the Reykjanes EXperiment

This paper presents a study of the sensitivity of numerically simulated precipitation across a mesoscale mountain range to horizontal resolution, cloud condensation nuclei (CCN) spectrum, initiation of cloud ice, numerical treatment of horizontal diffusion and initial and boundary conditions. The fifth generation Penn State/National Center for Atmospheric Research (PSU/NCAR) Mesoscale Model (MM5) is used in the study, in which the model is run at 8, 4 and 2 km horizontal resolutions and with a number of microphysical and numerical configurations. The model simulated precipitation is compared to the observed precipitation over the Reykjanes mountain ridge during the Reykjanes Experiment in Southwest Iceland in the autumn of 2002. Improvements in representation in topography at increasing horizontal resolutions yield large improvements in the accuracy of the simulated precipitation. At 8 km horizontal resolution the simulated maximum precipitation is too low, but the simulated precipitation upstream of the mountains is too high. The absolute values and the pattern of the precipitation field improve stepwise when going from horizontal resolutions of 8 km to 2 km, with the main contribution being when going from 8 km to 4 km. Calculations of diffusion and ice initiation do not seem to have a large impact on the simulated precipitation, which is on the other hand quite sensitive to the CCN spectrum. The simulations underestimate the precipitation over

the downstream slopes of the mountain ridge by factors of 2–3. There are indications that this underestimation may be associated with a systematic overestimation of downslope winds, and possibly descending motion, by the model.

4.4 Paper IV: Extracting statistical parameters of extreme precipitation from a NWP model

Precipitation simulations on an 8 km grid using the PSU/NCAR Mesoscale Model MM5 are used to estimate the M5 and C_i statistical parameters in order to support the M5 map used for flood estimates by Icelandic engineers. It is known a priori that especially wind anomalies occur on a considerably smaller scale than 8 km. The simulation period used is 1962–2005 and 73 meteorological stations have records long enough in this period to provide a validation data set. Of these only one station is in the central highlands, so the highland values of the existing M5 map are estimates. A comparison between the simulated values and values based on station observations set shows an M5 average difference (observed-simulated) of -5 mm/24 h with a standard deviation of 17 mm, 3 outliers excluded. This is within expected limits, computational and observational errors considered. A suggested correction procedure brings these values down to 4 mm and 11 mm, respectively.

4.5 Paper V: Validation of Numerical Simulations of Precipitation in Complex Terrain at high Temporal Resolution

Atmospheric flow over Iceland has been simulated for the period January 1961 to July 2006, using the mesoscale MM5 model driven by initial and boundary data from the ECMWF. A systematic comparison of results to observed precipitation has been carried out. Undercatchment of solid precipitation is dealt with by looking only at days when precipitation is presumably liquid or by considering the occurrence and non-occurrence of precipitation. Away from non-resolved orography, the long term means (months, years) of observed and simulated precipitation are often in reasonable agreement. This is partly due to a compensation of the errors on a shorter timescale (days). The probability of false alarms (the model predicts precipitation, but none is observed) is highest in N Iceland, particularly during winter. The probability of missing precipitation events (precipitation observed but none is predicted by the model) is highest in the summer and on the lee side of Iceland in southerly flows.

4.6 Paper VI: Dynamical Downscaling of Precipitation in Iceland 1961–2006

Atmospheric flow over Iceland has been simulated for the period January 1961 to July 2006, using the mesoscale MM5 model driven by initial and boundary data from the European Centre for Medium Range Weather Forecasts (ECMWF). Firstly, the simulated precipitation is compared to estimates derived from mass balance measurements on the Icelandic ice caps. It is found that the simulated precipitation compares favourably with the observed winter balance, in particular for Hofsjökull, where corrections to take liquid precipitation and/or winter ablation into account have been made, and for the outlet glaciers Dyngjujökull and Brúarjökull. Secondly, the model output is used as input to the WaSiM hydrological model to calculate and compare the runoff with observed runoff from six watersheds in Iceland. It is found that model results compare favourably with observations. Overall, the MM5 V3–7 is somewhat better than the MM5 V3–5. The V3–7 is drier than V3–5 on upstream slopes.

4.7 Paper VII: Downslope windstorm in Iceland – WRF/MM5 model comparison

A severe windstorm downstream of Mt. Öræfajökull in Southeast Iceland is simulated on a grid of 1 km horizontal resolution by using the PSU/NCAR MM5 model and the Advanced Research WRF model. Both models are run with a new, two equation planetary boundary layer (PBL) scheme as well as the ETA/MYJ PBL schemes. The storm is also simulated using six different micro-physics schemes in combination with the MYJ PBL scheme in WRF, as well as one "dry" run. Output from a 3 km MM5 domain simulation is used to initialise and drive both the 1 km MM5 and WRF simulations. Both models capture gravity-wave breaking over Mt. Öræfajökull, while the vertical structure of the lee wave differs between the two models and the PBL schemes. The WRF simulated downslope winds, using both the MYJ and 2EQ PBL schemes, are in good agreement with the strength of the observed downslope windstorm. The MM5 simulated surface winds, with the new two equation model, are in better agreement to observations than when using the ETA scheme. Micro-physics processes are shown to play an important role in the formation of downslope windstorms and a correctly simulated moisture distribution is decisive for a successful windstorm prediction. Of the micro-physics schemes tested, only the Thompson scheme captures the downslope windstorm.

Chapter 5

General discussions

5.1 Discussions on peer reviewed papers

In the first paper *Mapping of Precipitation in Iceland using Numerical Simulations and Statistical Modeling* (Rögnvaldsson et al., 2004) we presented our initial findings on the matter. The ten year simulations, run at 8 km horizontal resolution, were compared to the results of a statistical model based on observations, as well as observations for the same period. The initial results where promising as the atmospheric model did capture the observed precipitation pattern, as interpreted by the statistical model, in areas where there was good geographical coverage of rain gauges. The simulations also revealed plausible precipitation pattern in the data sparse high-lands, e.g. more precipitation in the mountains and a rain shadow in sheltered areas north of Vatnajökull ice cap (cf. Fig. 5.1 Compared to observations the model did overestimate precipitation in certain regions and more so during colder months. This lead us to speculate that part of the discrepancy was due to wind-loss of solid precipitation in the observations. It was also not clear for how large an area some of the observational sites, where precipitation was measured, were representative.

In light of these observational issues, in our next paper *Numerical Simulations of Precipitation in the complex Terrain of Iceland – Comparison with Glaciological and Hydrological Data* (Rögnvaldsson et al., 2007b), we compared simulated precipitation to accumulated winter precipitation on four ice caps and to simulated river-runoff. To be precise, the simulated precipitation, and other meteorological variables, were used as input to the WaSiM-ETH hydrological runoff model. The runoff, as simulated by the WaSiM-ETC model, was then compared to observed runoff from six watersheds. The simulation period was longer than for the first experiment (Rögnvaldsson et al., 2004), fifteen years instead of ten, but the simulation domain was kept unchanged. This extended simulation period allowed more focus to be put on investigating temporal trends in precipitation. The seasonal and inter-

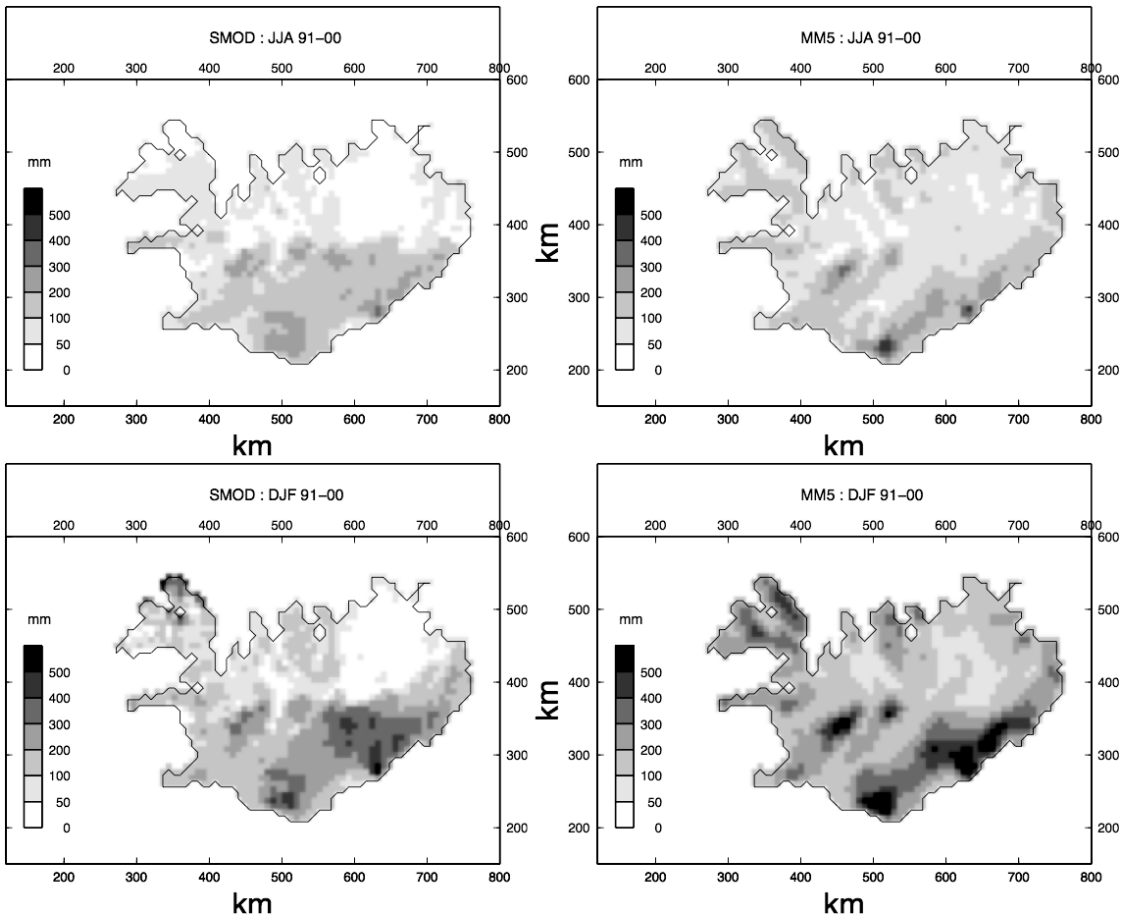

Figure 5.1: *Season average monthly precipitation for June, July, and August (JJA) 1991–2000 [mm] (top) and December, January, and February (DJF, bottom). Reference precipitation as simulated by the statistical model is shown on left panels and precipitation simulated by MM5 on the right panels. Same as Fig. 5 in Rögnvaldsson et al. (2004).*

annual variability of precipitation is investigated at low as well as high altitudes. The simulated precipitation (cf. Fig. 5.2) was found to be in good agreement with the two independent data sets used for comparison and generally within observational errors. In areas where there is substantial subgrid orography, changes in the horizontal resolution will inevitably lead to locally different simulated precipitation. Such a difference may, however, not give a proportionally large signal in tests of the kind that are presented in this paper. This is because the glacier observations are not in the vicinity of substantial subgrid variability in orography, and because the runoff calculations are all based on averaging over a large area. At 8 km horizontal resolution, the finer details of the orography are to some extent lost. This is especially true for geographical features where the ratio between mountain width and height is small, such as narrow ridges or stand-alone mountains. The Rögnvaldsson et al.

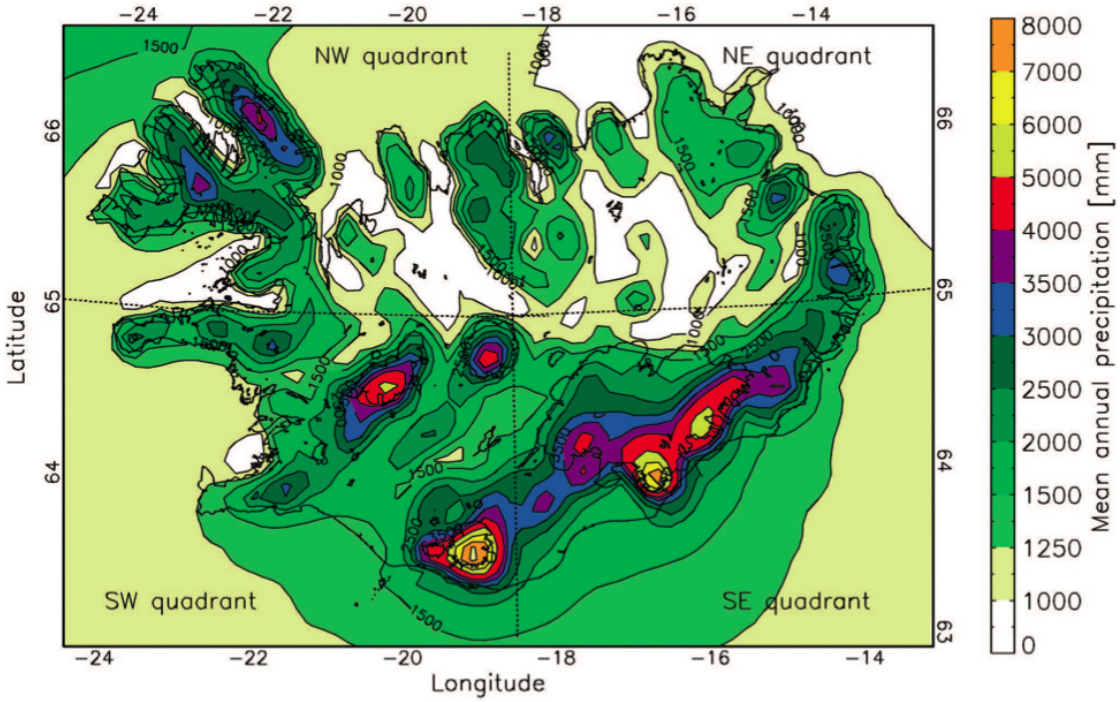

Figure 5.2: *Mean annual precipitation from March 1988 through February 2003 as simulated by the MM5 model. Dashed lines show the definition of NW, NE, SE and SW quadrants. Same as Fig. 7 in Rögnvaldsson et al. (2007b).*

(2007b) paper did therefore not address the question how increased model resolution would modify the precipitation pattern. However, in order to assess the impact of orography on the precipitation climate of Iceland, precipitation was simulated with flat Iceland and compared to a simulation with true orography for a one year period (cf. Fig. 5.3).

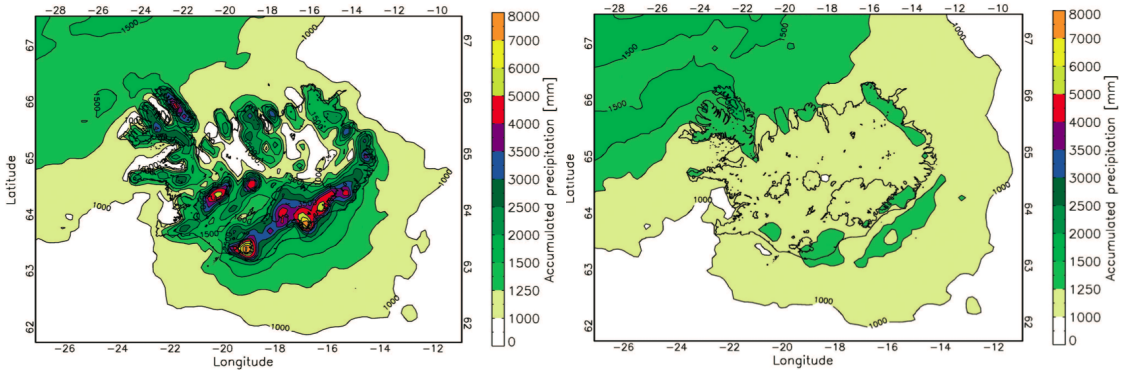

Figure 5.3: *Simulated precipitation [mm] for 2001–02 (September through August) with unmodified terrain (left) and with the orography reduced to one meter (right). Same as Fig. 11 in Rögnvaldsson et al. (2007b).*

In the third paper, *Sensitivity Simulations of Orographic Precipitation with MM5 and comparison with Observations in Iceland during the Reykjanes EXperiment* (Rögnvaldsson et al., 2007a), we did investigate the sensitivity of simulated precipitation to model resolution. Figure 5.4 shows the location of observational stations during the REX intensive observation periods (IOP's) as well as simulated precipitation at 4 km model resolution during IOP5. In addition a number of sensitivity

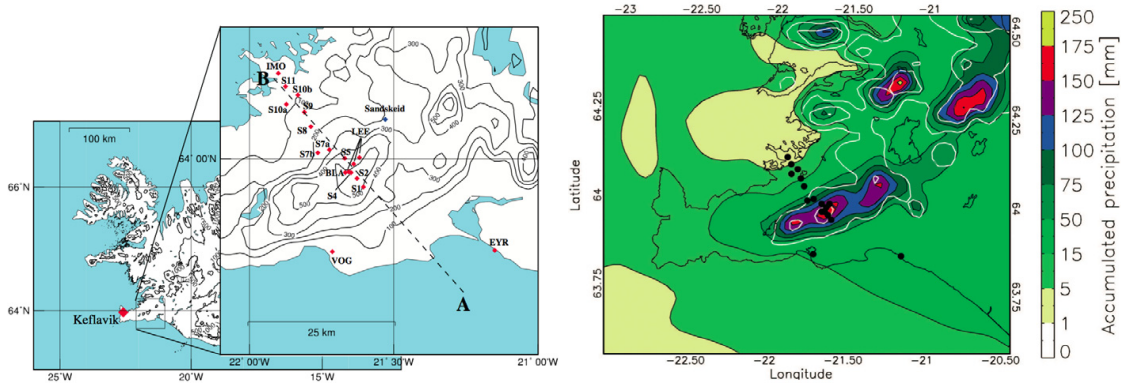

Figure 5.4: *Overview of station location during REX (left). Stations EYR (Eyrarbakki), VOG (Vogsósar), BLA (Bláfjöll), IMO (Icelandic Meteorological Office, WMO 4030) and Keflavík (WMO 4018) are part of the operational network in Iceland. Other stations, S1, S2, S4, S5, LEE (taken as mean of three stations), S7a, S7b, S8, S9, S10a, S10b and S11 were installed specifically for the Reykjanes EXperiment. Station Sandskeið is shown in blue. Topography is shown with height intervals of 100 meters. On the right, terrain and accumulated precipitation during IOP5 is shown, as simulated in the REX2_CNP30 run (cf. Table 1 in Rögnvaldsson et al. (2007a)). Contour lines (white) of the terrain are plotted every 250 meters. Location of observation sites are shown by black dots. Same as Figs. 2 (left panel) and 3 (right panel) in Rögnvaldsson et al. (2007a).*

tests where done in order to see how changes to the microphysical parameterizations would affect the simulated precipitation. The simulation results revealed most sensitivity to the CCN spectra (cf. Fig. 5.5), which in turn was tuned by modifying the droplet concentration, i.e. the minimum number of droplets per unit volume needed before warm rain condensation can be initiated. By modifying the microphysics scheme towards a more maritime climate, i.e. less droplet concentration per unit volume (equivalent to assuming larger droplets), resulted in simulated precipitation that was closer to observed values. The simulation showed limited sensitivity to changes made to how cloud ice was initiated and how horizontal diffusion was calculated. This indicates that the precipitation process, as modeled by the microphysics scheme, was to a large extent warm rain. Increasing model resolution did reveal large sensitivity, both for upslope precipitation (reduced when model reso-

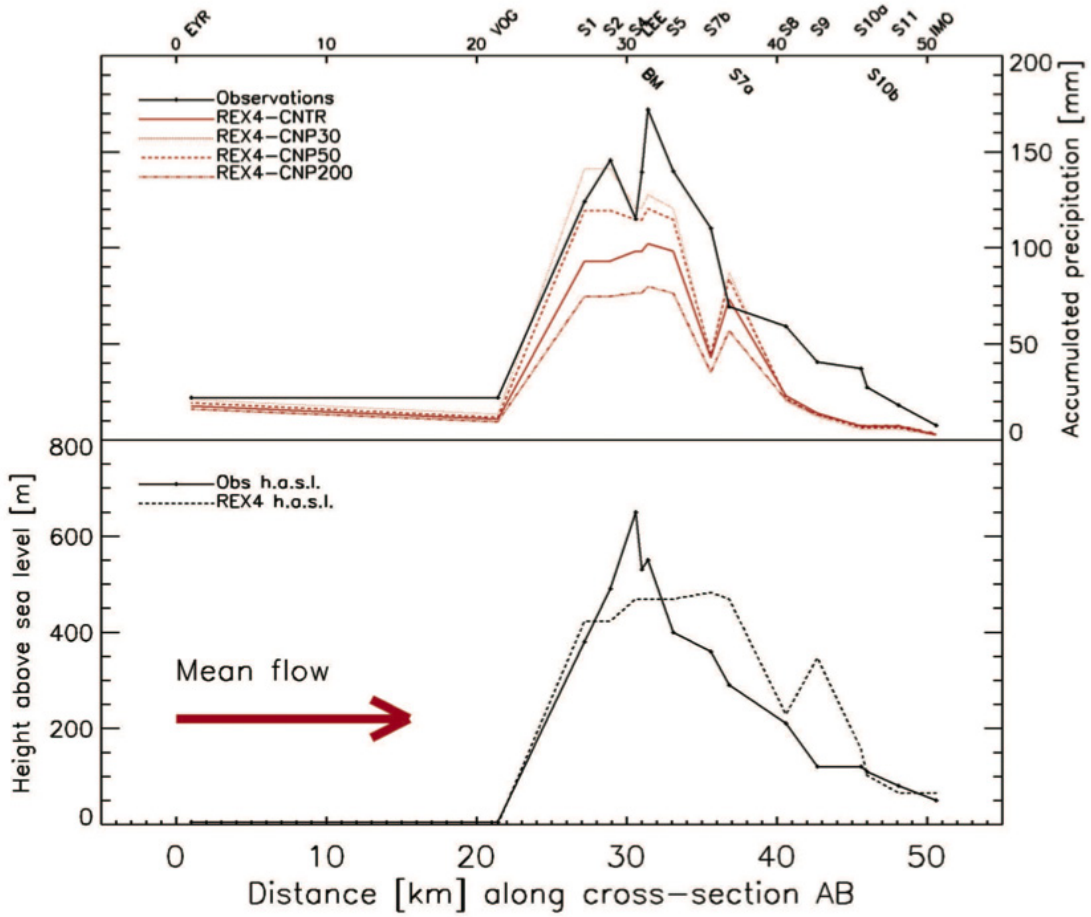

Figure 5.5: *Sensitivity to different values of CNP at 4 km horizontal resolution, CNP = 100 (CNTR, solid line), CNP = 30 (dotted line), CNP = 50 (dashed line) and CNP = 200 (dot-dashed line). Bottom panel shows the model and actual orography along cross section AB in Fig. 5.4. Same as Fig. 6 in Rögnvaldsson et al. (2007a).*

lution was increased) and precipitation at mountain crest (increased when model resolution was increased). All simulations did however underestimate precipitation downstream of the mountain. This behavior indicates that the model did indeed not capture the true quantity of solid hydrometeors, i.e. it underestimated the amount of ice being initiation and/or the amount of ice and snow being formed via various processes, such as aggregation. The reason is that solid hydrometeors (e.g. snowflakes) have much lower fall velocities than liquid drops. These hydrometeors can therefore be advected by the flow, in this case over the mountain ridge. Another possible reason for the lee-side dryness is too much downdraft, leading to an overestimation of evaporation. Comparison with observations did indeed reveal overestimation of surface winds on the lee-side of the mountain ridge. The results from this study indicate that the precipitation mapped at 8 km resolution as in

Bromwich et al. (2005) and Rögnvaldsson et al. (2004, 2007b) gives too small maxima over the mountain crest and far too little precipitation directly downstream of the crest. This can have considerable economical implications, as the spatial distribution of precipitation plays a key part in planning and use of water resources.

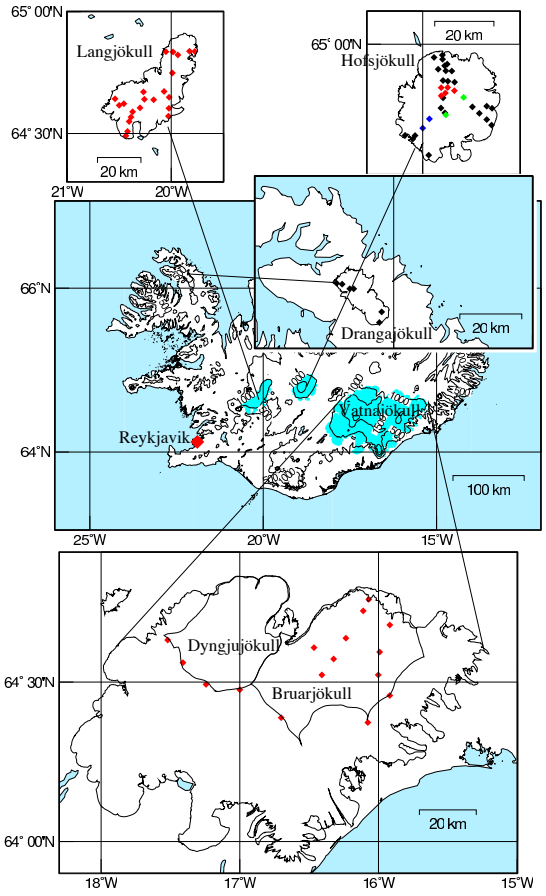

Figure 5.6: *Overview of the six ice caps and glaciers used for validation purposes, where dots indicate a typical location of an observation site. Red dots on Hofsjökull glacier are along profiles HN (N part), blue dots along profile HSV (SW part) and green dots along profile HSA (SE part). Observations at locations shown in black at Hofsjökull have not been used in this study. Drangajökull is split up in two regions, NW and SE parts (cf. Table 2 in Rögnvaldsson et al. (2010)). See Figure 1 in Rögnvaldsson et al. (2007b) for comparison. Same as Fig. 2 in Rögnvaldsson et al. (2010).*

In the sixth paper, *Dynamical Downscaling of Precipitation in Iceland 1961–2006* (Rögnvaldsson et al., 2010), we extended the study presented in Rögnvaldsson et al. (2007b). The simulation period was considerably longer than in the earlier investigation, or 45 years. This gave us the opportunity to extend the simulated runoff series and compare to earlier observations, more glaciological data was also available (cf. Fig. 5.6). In this study a newer version of the MM5 atmospheric model was used (version 3.7 vs. version 3.5 in earlier studies). The simulated precipitation was again compared to non-conventional observations of precipitation, i.e. snow accumulation and runoff. As before, the simulated precipitation did compare favorably with observations. There where noticeable differences from the earlier simulation for the overlapping 15 year period 1987–2003 (cf. Fig. 5.7). Most notably the newer version of MM5 simulated less precipitation on the upstream slopes of mountains that are well represented at the model horizontal resolution. This is believed to be caused by changes made in the microphysics scheme used (the Reisner2 scheme, (Reisner et al., 1998)). Notably, version 3.5 of MM5, used in Rögnvaldsson et al. (2007b)

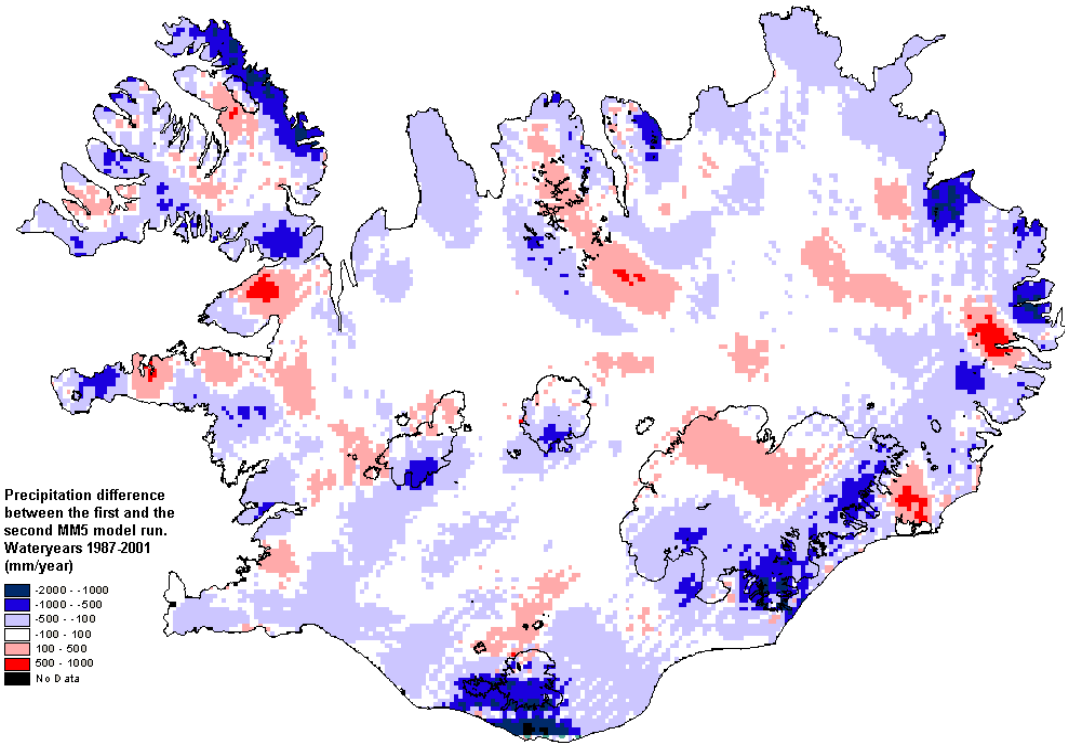

Figure 5.7: *Difference (MM5 V3.7 minus MM5 V3.5) in simulated mean annual precipitation for the water years 1987–2002. Same as Fig. 8 in Rögnvaldsson et al. (2007b).*

used the Kessler autoconversion[1] scheme. As of version 3.6 of MM5, this scheme was swapped with that of Berry and Reinhardt as implemented by Walko et al. (1995). The Kessler scheme has been known to produce too much precipitation upstream of mountains. The glaciological and runoff data only provides validation on a much longer timescale than conventional rain-gauge data, and the daily error in the precipitation downscaling remains unclear. However, the comparison with the observational data shows that the climatological values of the simulated precipitation are of good quality.

The temporal and spatial accuracy of precipitation simulated in Rögnvaldsson et al. (2010) was investigated for the period 1987–2003 in the fifth paper *Validation of Numerical Simulations of Precipitation in Complex Terrain at high Temporal Resolution*, (Arason et al., 2010). The main findings where that away from non-resolved orography, long term (months, years) sums of simulated precipitation are quite correct in the south but too high in the north. This was partly due to compensating errors on a smaller timescale (days). Figure 5.8 shows the relative

[1] Autoconversion is the process where cloud droplets collide and coalesce with each other and eventually form raindrops.

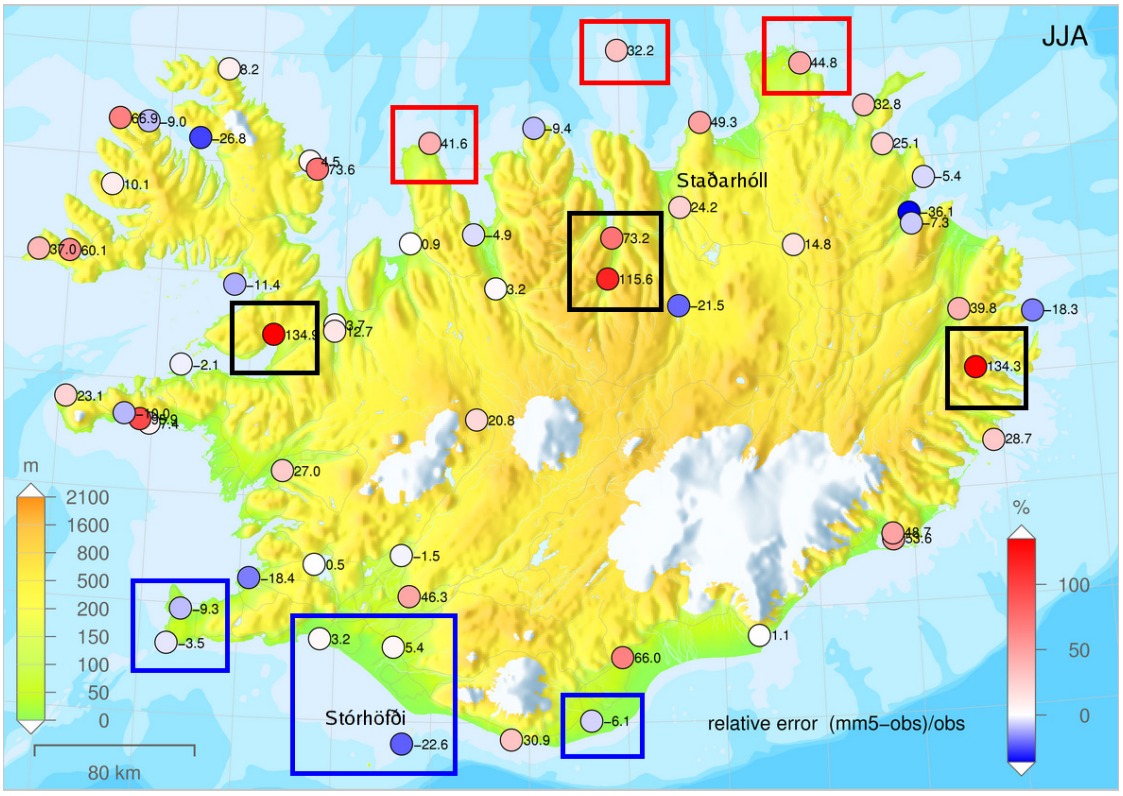

Figure 5.8: *A topographic map of Iceland showing relative difference between simulated and observed accumulated precipitation, (mm5-obs)/obs, in June, July and August (JJA). Each colored circle corresponds to a synoptic weather station. Station names are included at the stations referred to in the Arason et al. (2010) paper. The color of the circle denotes the relative error in the simulations (colorbar to the right). The blue boxes enclose a few stations on flat land in S Iceland where the observations and simulations are in reasonable agreement. The red boxes draw attention to stations in N Iceland where the model overestimates precipitation, despite these stations being on flat land. Stations that have huge overestimation, which is almost certainly due to non-resolved orography, are enclosed in black boxes. Same as Fig. 1 in Arason et al. (2010).*

difference between simulated and observed accumulated precipitation during the summer months June, July, and August for the period 1987–2003. The probability of false alarms (the model predicts precipitation, but none is observed) is highest in N Iceland, particularly during winter. The probability of missing precipitation events is highest in the summer and on the lee side of Iceland in southerly flows. Precipitation is underestimated in southeasterly flows at the SW coast of Iceland and is overestimated at the N coast of Iceland. This cannot only be explained by non-resolved orography.

In spite of the shortcomings of the downscaled precipitation demonstrated in

Arason et al. (2010), it is still possible to gain valuable statistical information from the data set. The fourth paper, *Extracting statistical parameters of extreme precipitation from a NWP model*, (Elíasson et al., 2009), demonstrates just that. In this paper the authors use the simulated precipitation from Rögnvaldsson et al. (2010) to estimate the M5 and C_i statistical parameters in order to support the M5 map used for flood estimates in Iceland.

In the seventh paper, *Downslope Windstorm in Iceland – WRF/MM5 Model Comparison*, (Rögnvaldsson et al., 2011), we take a closer look at a severe windstorm in SE Iceland. In this study we compared the MM5 and WRF models. Both models are run with a new, two equation planetary boundary layer (PBL) scheme as well as the ETA/MYJ PBL schemes. The storm was also simulated using six different micro-physics schemes in combination with the MYJ PBL scheme in WRF. The new two equation PBL scheme, when implemented within the MM5 model, did capture the downslope windstorm better than the ETA scheme. There was however less difference seen between the two WRF simulations, i.e. the one using the MYJ scheme and the two equation scheme. The sensitivity tests using different micro-physics scheme revealed that thermodynamical processes can play a very important role in the formation of downslope windstorms. Forced ascend, or descend, can cause changes in phases of hydrometeors and hence modifications in the temperature field via release (or uptake) of heat due to the phase changes. This change in temperature can in turn modify the stability of the impinging flow, and as explained by e.g. Durran (1990), upslope stability at mountain height can be a crucial factor in the formation of a downslope windstorm.

5.2 Climatology of winds

A preliminary study on surface winds from a fifteen year period (1987–2002) of simulated MM5 data was done by Rögnvaldsson and Ólafsson (2005a). In this study observations from thirteen stations where compared to simulated winds (cf. Fig.5.9). The stations were both near the coast and at higher altitudes. Two points show the greatest discrepancies, stations Stórhöfði and Reykjavík. The anemometer at Stórhöfði is on a 120 meter high cliff whilst the corresponding grid cell in MM5 is at sea level. This discrepancy between the topography in the model and reality explains the large difference between the measured (10.4 m/s) and simulated (7.6 m/s) wind speed. The Reykjavík weather station is at 50 meter altitude but the nearest model grid cell is at 150 meter altitude. There is further a strong coastal gradient in the wind field, the next inland grid cell having considerably less wind speed (5.7 m/s).

In this study the authors conclude that the simulated wind speeds agreed fairly well with observations and that the observed discrepancies could to a large extent

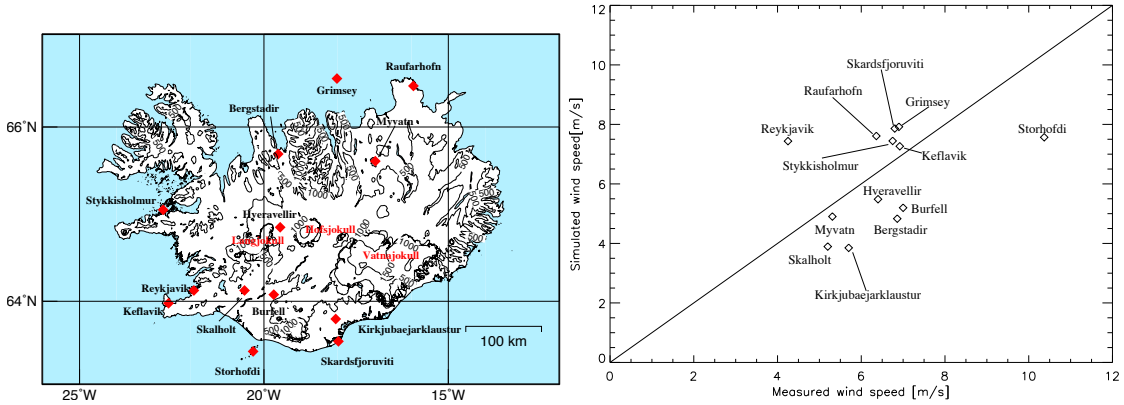

Figure 5.9: *Observation stations (red diamonds) used for comparison with the MM5 simulations (left panel) and comparison between measured (x-axis) and simulated (y-axis) annual mean wind speed at the thirteen observation sites (right panel). Same as Figs. 1 (left) and 4 (right) in Rögnvaldsson and Ólafsson (2005a).*

be explained by the model coarse resolution and corresponding errors in land use parameters and orography. Another source of discrepancies was the inherited uncertainty of anemometers. The authors further speculated that too little mixing near the surface in the PBL scheme used could have contributed to too low simulated wind speeds in the interior of Iceland.

Long term downscaling experiments have also been done using the WRF atmospheric model, both version 2.2 and 3.0.1. These simulations range from fall 1957 to spring 2011 and 2012, respectively. Data from the older version of WRF, which was run at a 9 km horizontal resolution, have been used to calibrate a runoff model developed by the Vatnaskil Engineering company[2]. This runoff model is now being driven in operational mode with data from an ensemble forecasting system operated by IMR. The resulting runoff data are in turn used for day-to-day decision making at Landsvirkjun, Iceland's largest electrical power producer. The series created with version 3.0.1 of WRF was run at a 27 km resolution for the period September 1957 to September 2009. The model was also run at a 9 km resolution for the whole 1957–2012 period, and at a 3 km resolution for the period 1994–2012, using one-way nesting in on-line mode. A further 1 km domain was run for part of S Iceland for the seven year period September 2002 to September 2009. The various model domains are shown in Fig. 5.10. The model was run with the two equation PBL scheme discussed earlier and described in detail in Bao et al. (2008). Table 5.1 shows the various parameterization schemes used for the two downscaling experiments. Comparisons of the heights of various pressure levels, wind speed and direction, and temperature with upper air observations at Keflavík airport show that the large scale flow is well captured by the simulations (cf. Fig. 5.11).

[2]http://www.vatnaskil.is

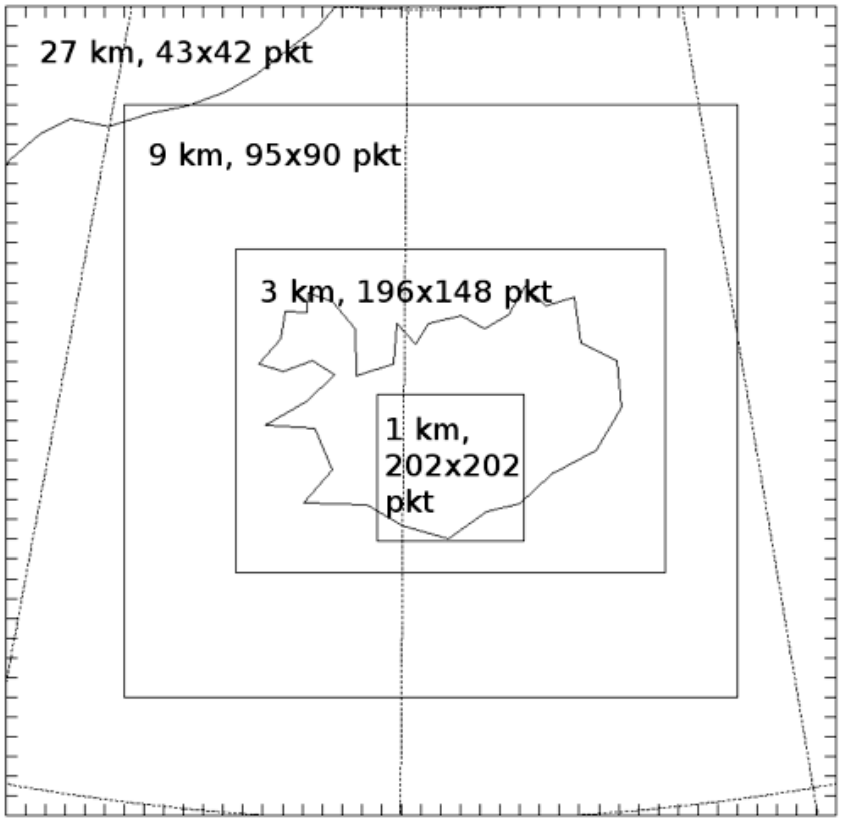

Figure 5.10: *WRF domain configurations for the various downscaling experiments of ERA-40 and ECMWF re-analysis data. The 9 and 3 km domains are the same for both version 2.2 and 3.0.1 simulations but the 27 and 1 km domains were only used with version 3.0.1.*

Table 5.1: *Various parameterization schemes used for dynamical downscaling experiments using two different versions of the WRF model.*

Parameterization scheme	**Version 2.2**	**Version 3.0.1**
Microphysics	Thompson graupel	Thompson graupel
Cumulus	Kain-Fritsch	Betts-Miller-Janjic
Planetray boundary layer	Mellor-Yamada-Janjic	Two equation
LW radiation	RRTM	RRTM
SW radiation	Dudhia	Dudhia
Surface physics	NOAH LSM	NOAH LSM
Surface layer physics	Monin-Obukhov	Monin-Obukhov

Comparison of surface observations of wind direction, wind speed and temperature

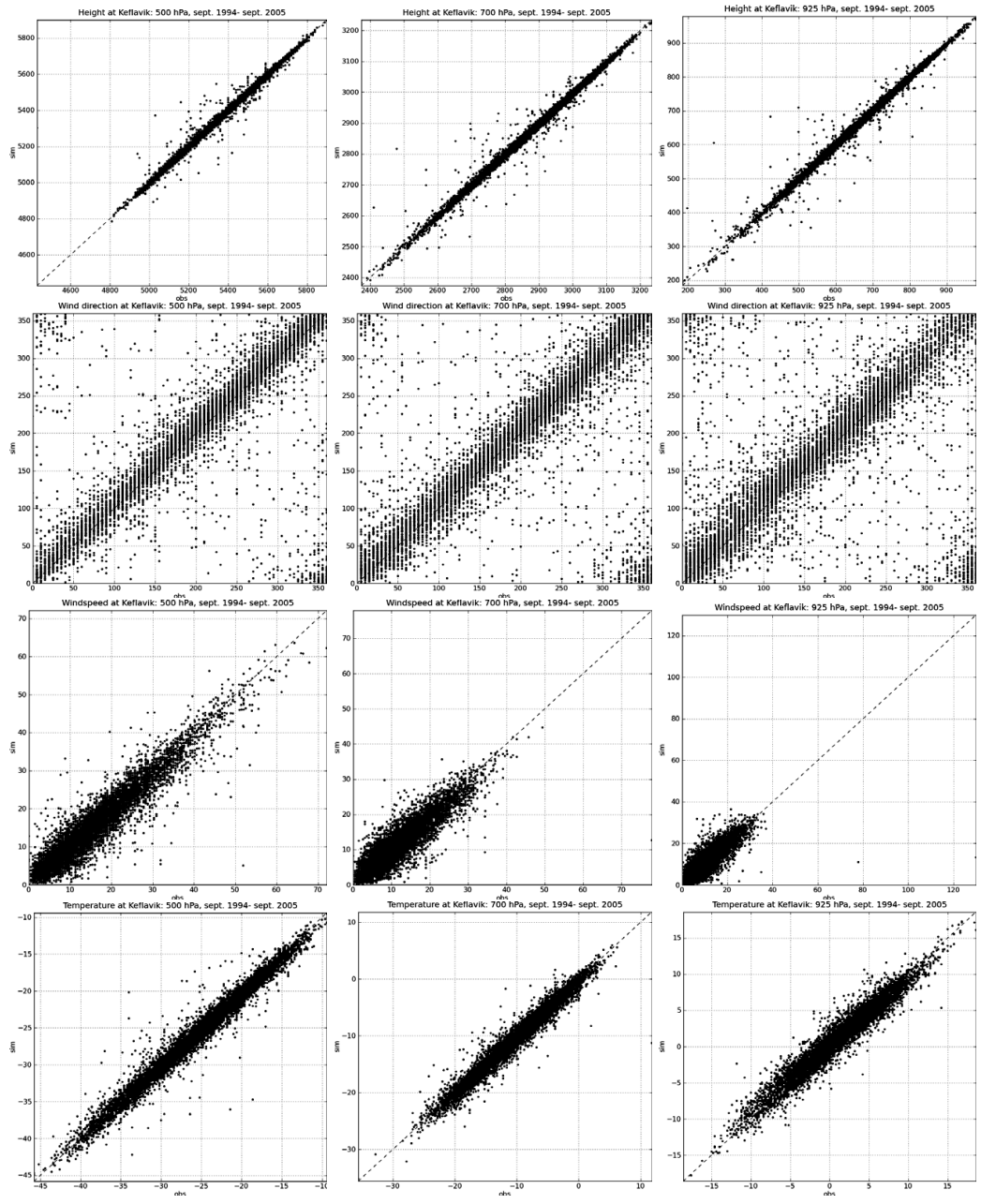

Figure 5.11: *Comparison of observed 500, 700, and 925 hPa heights (top) [m], wind direction (second from top) [°], wind speed (second from bottom) [m/s] and temperature (bottom) [°C] at 500 (left), 700 (middle) and 925 hPa (right). Horizontal axis shows observations and vertical axis simulated results at 3 km resolution. The comparison period is from September 1994 until September 2005 (both months included).*

with simulations are also favorable (cf. Fig. 5.12).

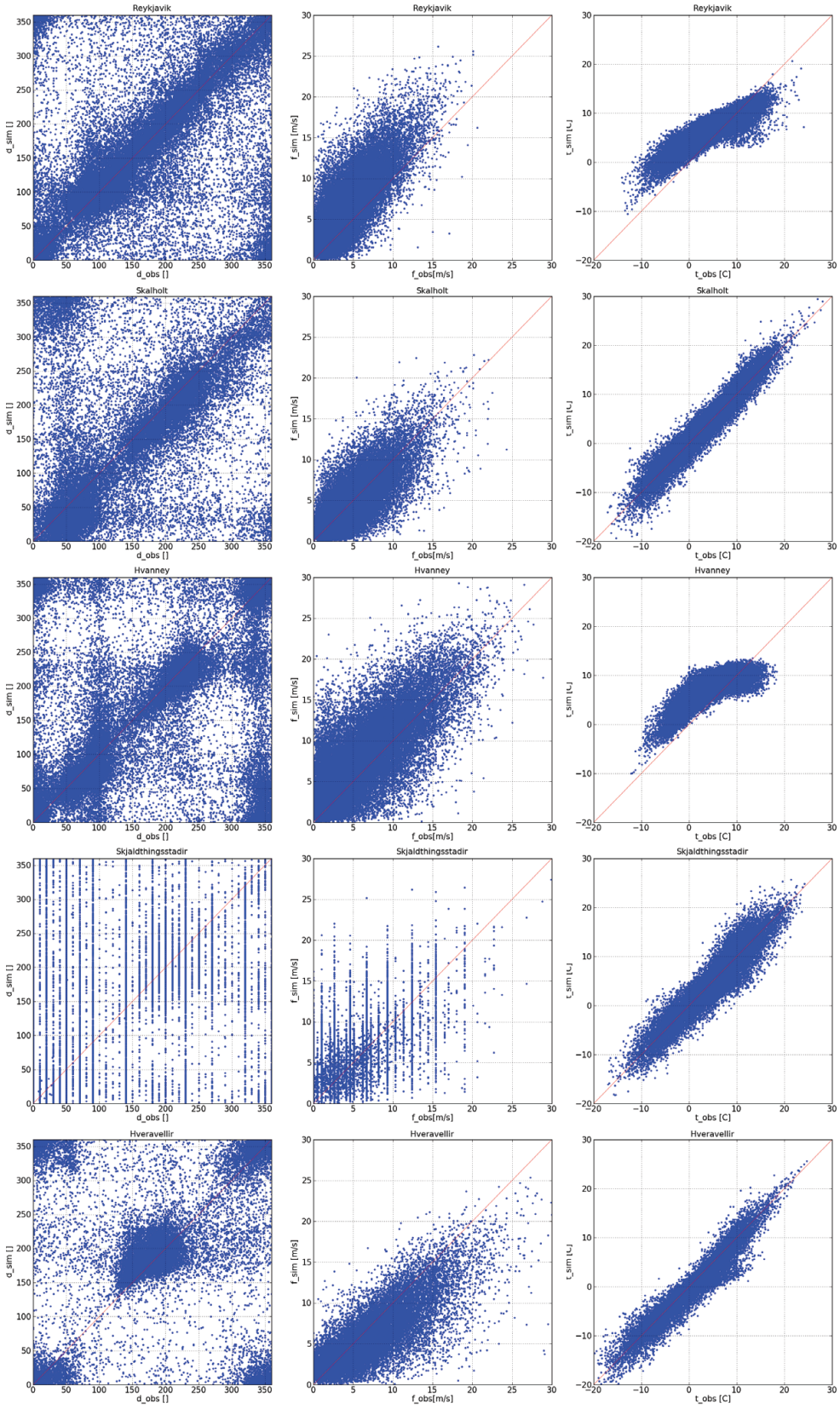

Figure 5.12: *Comparison of observed ten meter wind direction (left) [°] and wind speed (middle) [m/s], and two meter temperature (right) [°C] at Reykjavík (top), Skálholt (second from top), Hvanney (middle), Skjaldþingsstaðir (second from bottom), and Hveravellir (bottom). Horizontal axis shows observations and vertical axis simulated results at 3 km resolution. The comparison period is from September 1994 until September 2005 (both months included).*

Observed errors at various stations can, to some extent, be explained by:

- Sub-grid orography.
- Proximity to water bodies.
- Inaccurate landuse characteristics, e.g. incorrect surface roughness.

The 10 meter mean winds are shown for different classes of sub-periods in Figures 5.13 to 5.15. The patterns revealed in these figures correspond to features

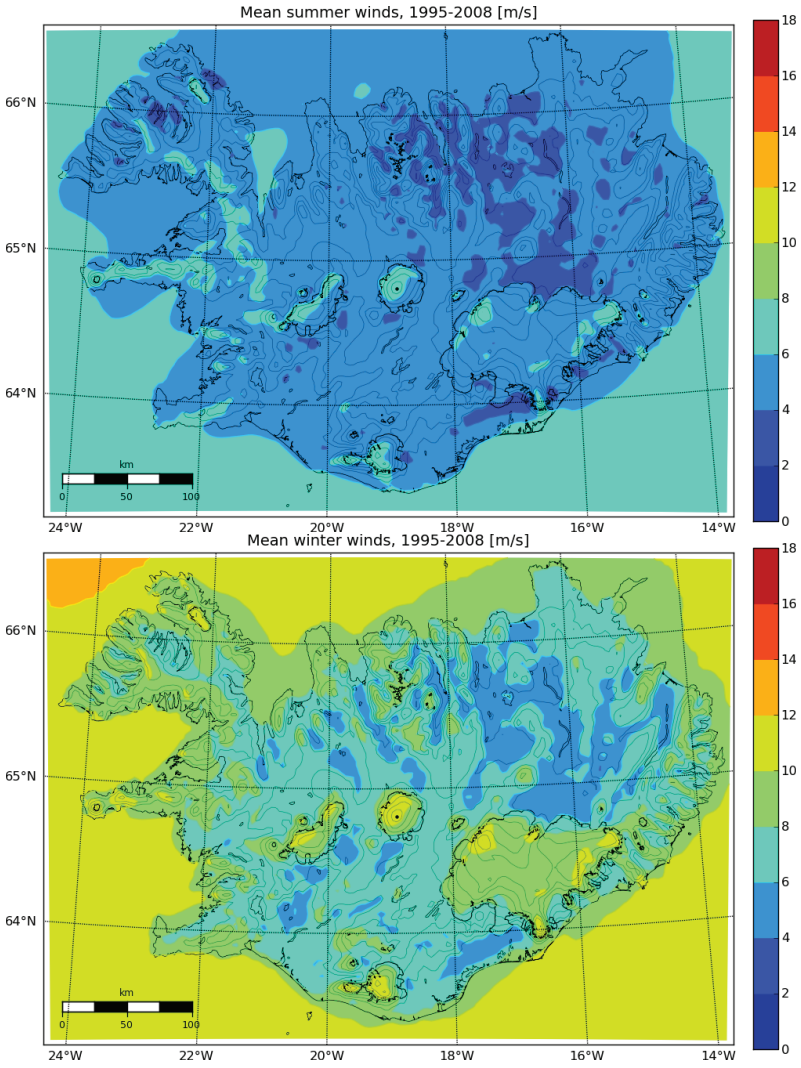

Figure 5.13: *Simulated mean summer (June, July, and August) ten meter windspeed (top) and winter (December, January, and February) windspeed (bottom) [m/s] for the period 1995–2008 (both years included).*

produced in flows at high Rossby numbers and values of Nh/U close to unity or above (upper central and upper right parts of the mountain wind diagramme in Fig. 3.5). In this parameter space, strong winds can be expected where the flow

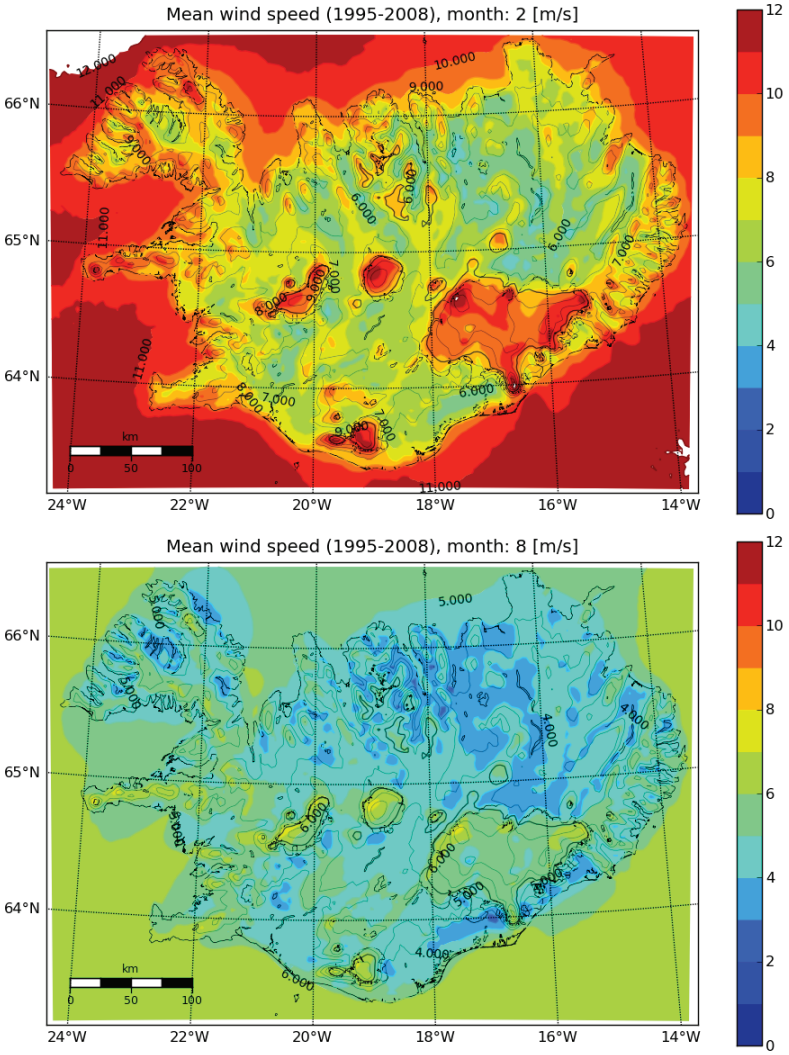

Figure 5.14: *Simulated mean monthly ten meter windspeed [m/s] for February (top) and August (bottom) for the period 1995–2008 (both years included).*

escapes past mountain ranges (corner winds) and above the downsream slopes of mountains. Weak winds are immediately upstream (blockings) and downstream (wakes) of mountains. At the scale of Iceland as a whole, the Coriolis force has an significant impact on the flow pattern. Here, we move downwards in the right part of the diagramme in Fig. 3.5 to intermediate or low Rossby numbers. In this parameter space, there is speed-up on the left side of the mountains. This speed-up may explain that the mean winds are stronger along the south coast than along the

north coast of Iceland. Winds from the SE, E and NE are much more frequent than winds from the westerly directions. The easterlies accelerate at the south coast, while the infrequent westerlies accelerate at the north coast. Figure 5.15 illustrates this effect nicely with a speed-up at the SW-coast in flow from the SE. In the mean

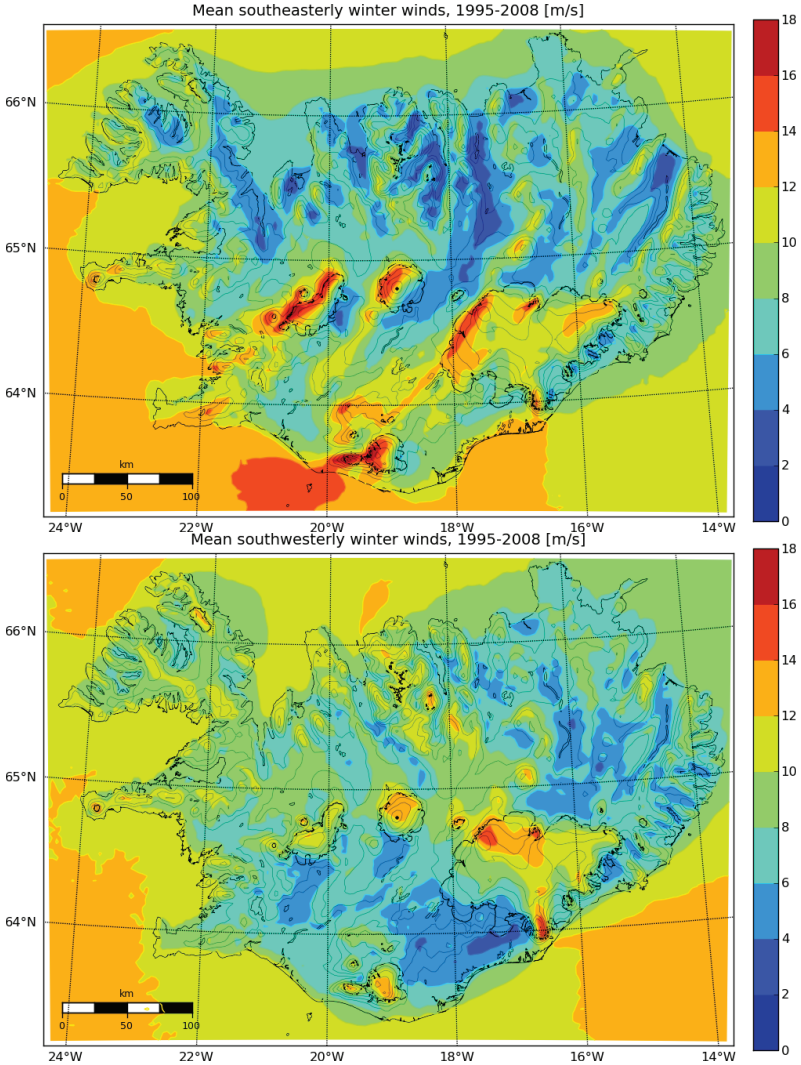

Figure 5.15: *Simulated mean ten meter windspeed [m/s] for southeasterly (top) and southwesterly (bottom) winds for the winter (January, February and March) months for the period 1995–2008 (both years included).*

flow, areas of strong winds in the mountains are not above the mountain tops, but in the western slopes. This suggests strong persistency of gravity waves in easterly winds. This pattern becomes particularly clear in winds from individual directions as in Fig. 5.15.

In the winter, the difference between mean wind speed in the lowlands and over

the ocean is much greater than in the summer. This difference reflects the high static stability of the winter boundarylayer over cold land surface, compared to low static stability over the relatively warm ocean. In the summer, the situation is opposite; the ocean surface is often colder than the overlying airmass, while the daytime surface over land is in general warmer than the airmass, leading to lower static stability over land than over the ocean. Low static stability leads to much vertical miximg of momentum and consequently, the mean summer winds are only a little weaker over land than over the sea, while in the winter the mean winds at sea are much greater than inland.

Comparing flow from SE and flow from SW (cf. Fig. 5.15), the SE-flow features much stronger gravity-wave signal and weaker mean winds in N-Iceland (wake). Both these features may be attributed to higher static stability (and Nh/U) in winds from the SE than in winds from the SW. The flow from SE is often associated with advection of warm air ahead of an extratropical cyclone, while the flow from the SW is often associated with outbreak of a cold airmass over relatively warm ocean.

5.3 Dynamical downscaling of future climate

Rögnvaldsson and Ólafsson (2005b) investigated two simulations of future climate, focusing on Iceland and surrounding waters. The simulations were done with the numerical model HIRHAM (a version of the NWP model HIRLAM) at a horizontal resolution of 0.5° and with boundary conditions from global simulations by the Hadley centre, based on scenarii A2 and B2. The study indicated that precipitation in a future climate might increase substantially in NE-Iceland during mid-winter and mid-summer and in S-Iceland in the autumn. The simulated precipiation increase in mid-winter and autumn was found to be much greater in the mountain slopes than at the coast, indicating that a future climate might have a new and different precipitation change with height.

As part of the Nordic CES (Climate and Energy Systems) and Icelandic LOKS (LOfthjúpsbreytingar og áhrif þeirra á orkuKerfi og Samgöngur) projects (Thorsteinsson and Björnsson, 2012) we have used the WRF model to dynamically scale down simulations of both control period and future climate. In order to assess the impact of horizontal resolution on the simulated climate, the atmosphere has been simulated for selected areas at different resolutions (cf. Fig. 5.16). The forcing data are from the Bjerknes climate model, run at the Bjerknes Centre for Climate Research[3] (BCCR) in Bergen, Norway. Two periods were chosen, a control period 1961–1990 and a future period 2020–2050.

The modeling approach used in this experiment is that of Giorgi and Mearns (1999), i.e. we opt for a very large MOAD and long simulation times (one year).

[3] http://www.bjerknes.uib.no/

The atmosphere model used by BCCR is the Arpege model (Déqué et al., 1994), run

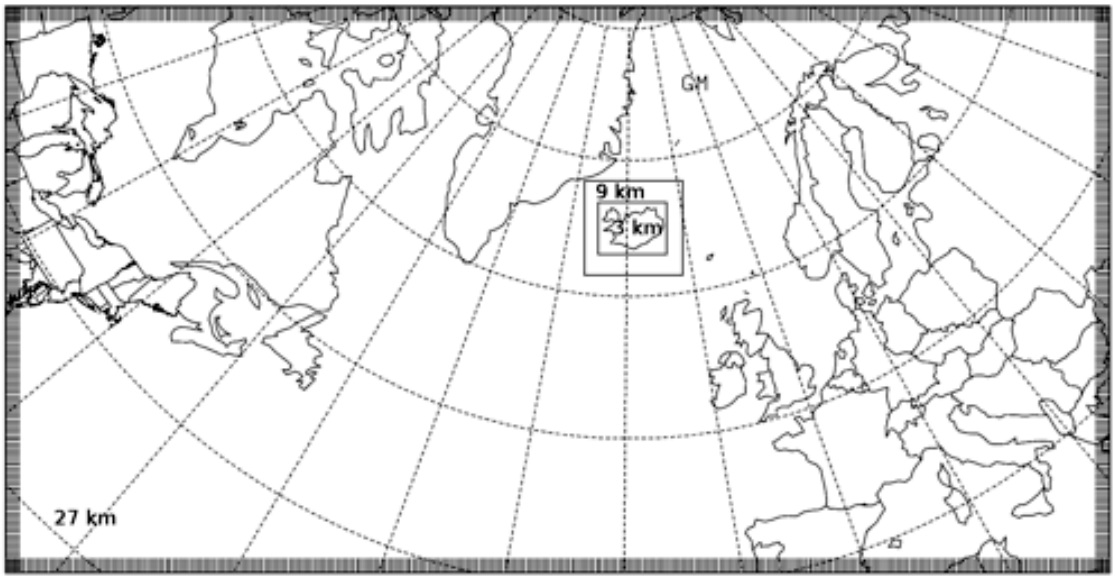

Figure 5.16: *WRF domain configurations for the Arpege control and future climate downscaling experiments. The outermost 27 km MOAD is 400×200 points, the 9 and 3 km domains covering Iceland are 94×91 and 196×148 points, respectively.*

on a T159c3 irregular grid. The scenario chosen was the SRES A1B (Nakićenović et al., 2000).

Prior to being pre-processed be the WRF model the Arpege data were regridded to a regular $1.125^\circ \times 1.125^\circ$ grid. The reason for this relatively coarse resolution was to prevent the creation of spurious high frequency noise by the regridding process in areas far from the high resolution part of the original Arpege simulation.

5.3.1 Results

The model resolution has a big impact on the simulated precipitation (cf. Fig. 5.17).

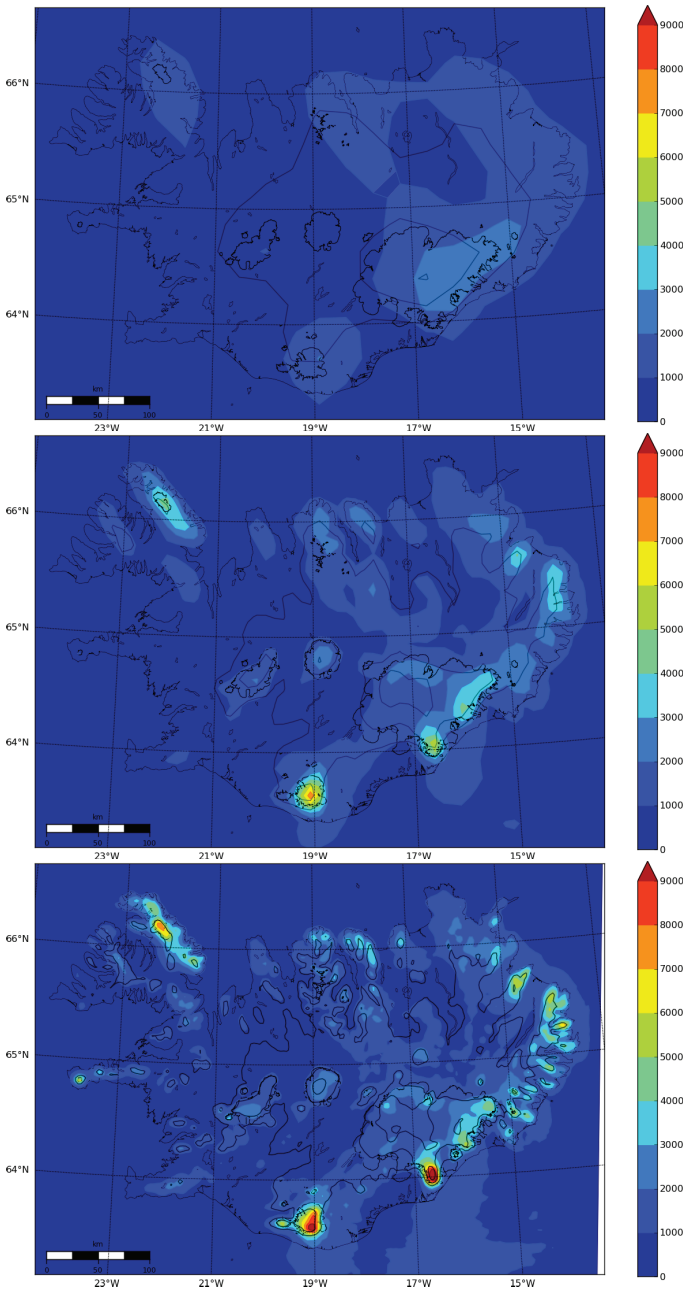

Figure 5.17: *The simulated annual precipitation [mm] for the period 2020 to 2021 increases as the horizontal resolution goes from 27 (top), to 9 (middle) and 3 km (bottom).*

As the model resolution is increased the terrain is better represented and the max-

imum precipitation values increases. The precipitation pattern also becomes more realistic and detailed, with high values in mountainous regions and over the large ice caps in S-, SE-, and Central Iceland. Comparison of simulated precipitation from this particular future climate scenario with the control period reveals both spatial and temporal changes. There is less annual precipitation in W-, SW-, and E-Iceland but more in SE- and Central Iceland (cf. Fig. 5.18). This pattern is even more pronounced for large events (not shown).

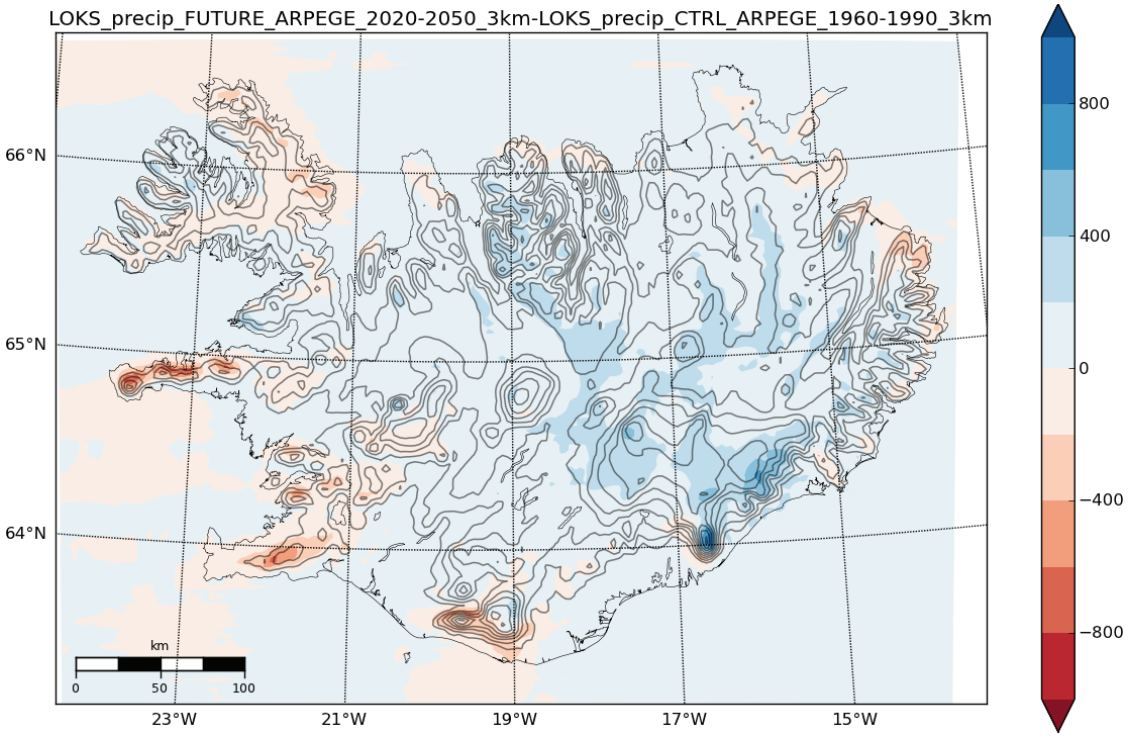

Figure 5.18: *Difference in simulated mean annual precipitation for the period 2020–2050 and 1960–1990 (future minus control).*

There are also signs of seasonal changes in the precipitation pattern, in particular for heavy precipitation events. Figure 5.19 shows a histogram of daily precipitation, separeted into different bins. There is little change in light precipitation events, but as daily precipitation increases there is a clear shift from winter and spring to summer and fall.

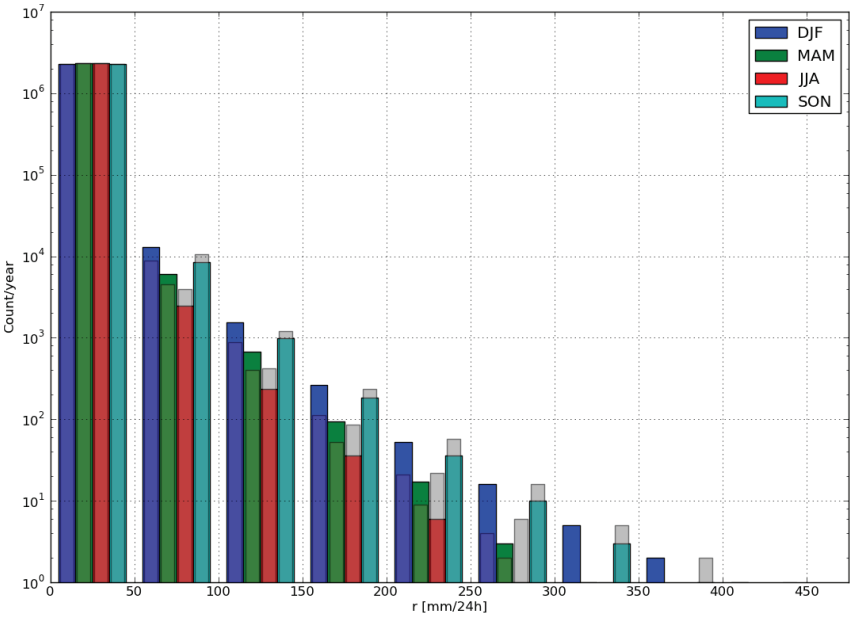

Figure 5.19: *Difference in simulated precipitation for the period 2020–2050 and 1960–1990 for different daily amounts, simulated at 3 km resolution. Vertical axis shows the number of grid cells within each precipitation amount bin shown on the horizontal axis. The control period is shown with coloured bars (different color for each three month period) and the future period is shown with shaded, slightly narrower bars.*

This trend can also be seen at 9km resolution, cf. Fig. 5.20. These seasonal vari-

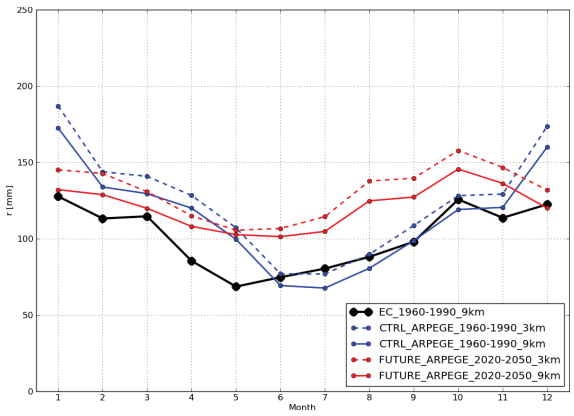

Figure 5.20: *Annual cycles of monthly mean precipitation for the control (red) and future (blue) periods at 9 (solid lines) and 3 (dashed lines) km resolution. The black line shows the same, but for the downscaled ERA40 data set at a 9 km resolution.*

ations in precipitation are not seen when looking at the 15-member multi-model ensemble mean changes from the CES (Thorsteinsson and Björnsson, 2012) project

(cf. Fig.5.21). These result indicate an increase in precipitation in future climate,

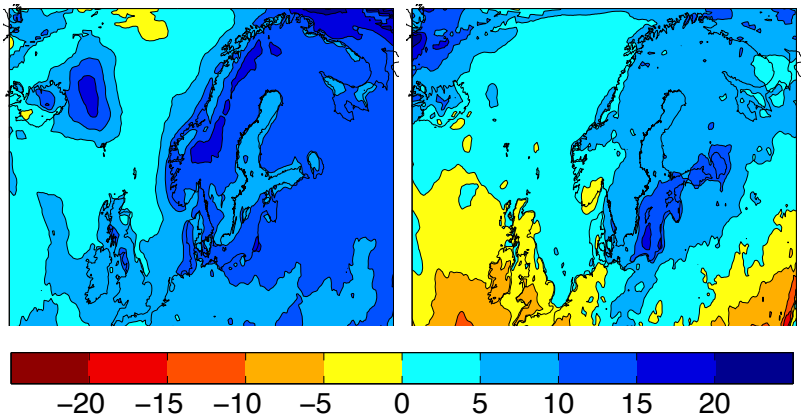

Figure 5.21: *Change in precipitation (%) in DJF (left panel) and JJA (right panel) comparing 2021–2050 with 1961–1990 (future minus control) for the 15-member multi-model ensemble mean from the CES project. Adapted from Fig. 3.1 in Thorsteinsson and Björnsson (2012).*

regardless of season. However, when one looks at results from individual scenario simulations the picture is quite different. Figure 5.22 shows relative changes in

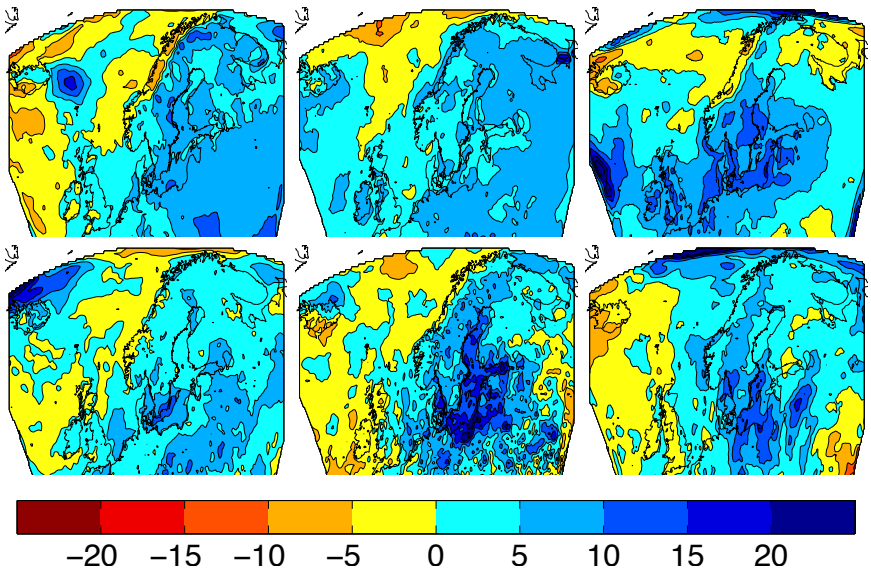

Figure 5.22: *Change in precipitation (%) in DJF (top panel) and JJA (bottom panel) comparing 2021–2050 with 1961–1990 (future minus control) for the DMI-HIRHAM-ECHAM5 (left), Met.No-HIRHAM-HadCM3Q0 (middle), and SMHI-RCA3-BCM simulations from the CES project. Same as Fig. 3.3 in Thorsteinsson and Björnsson (2012).*

precipitation for the three so-called recommended CES scenarios (cf. Table 3.1 in Thorsteinsson and Björnsson (2012)). These three reference simulations show considerable variability, both seasonal and spatial, with no clear consencus.

Similar seasonal variations, albeit for wind, have been reported for Ireland in Nolan et al. (2012). In this paper the authors use the COSMO-CLM model to scale down future climate scenarios (i.e. A1B and B1) from the ECHAM5. From a tvelwe member ensamble the authors conclude that the simulations show a marked increase in the amplitude of the annual cycle in wind strength with 9–13% more energy available during winter and 5–8% less during summer.

Chapter 6

General conclusions

Let us now restate our original research questions:

- Can one use a regional model to dynamically scale down a coarse resolution global atmospheric analysis to gain better understanding of temporal and spatial distribution of winds and precipitation in Iceland?
- What, if anything, is gained by increasing the horizontal resolution of the regional model?

As we have shown, than the answer to the first question is a definite "yes". The climate of Iceland is to a large extent governed by synoptic scale flow that impinges the topography. Both the flow and the topographical influence are relatively predictable. Therefore, this downscaling approach may work better for Iceland and surrounding waters, than for places with less predictable weather.

As for the second question, much additional information can be gained on both temporal and spatial variability of winds and precipitation by increasing the model resolution. The validity of model results is however strongly dependent on the quality of the initial atmospheric analysis and the ability of the model to correctly resolve the relevant physical processes, as well as parameterize the relevant sub-grid processes.

There are also limits to at which horizontal resolution current atmospheric models can operate. We will address these, and other eminent problems that emerge as one increases horizontal model resolution below 1 km, in the final chapter of this thesis.

Our main findings can be summarized as follows:

- Improvements in representation of topography in the numerical system lead to large and clear improvements in the accuracy of the simulated precipitation. This is both important for short range weather forecasts as well as for dynamical downscaling of past, present, and model scenarios of future climate.

- High resolution simulations are a useful and valuable tool to describe the temporal and spatial pattern of precipitation in the complex terrain of Iceland. A new methodology has been successfully applied:

  Validation of simulated annual precipitation with independent hydrological data from many watersheds.

  Validation of simulated winter precipitation by comparison with comparison of observed accumulated snow on a number of large ice caps.

- On a timescale of a day, or less, there are still substantial errors in simulated precipitation. Results on larger timescales (30 days and beyond) are better, but this is due to compensating errors on shorter timescales.

- The MM5 numerical simulations underestimate systematically precipitation immediately downstream of narrow (10 km) mountain ridges, independent of model resolution (8, 4, or 2 km). This underlines the need for high resolution observations of the atmospheric flow in the vicinity of the mountain ridge, as well as of the microphysical parameters.

- In spite of errros on short time scales, the numerical output is of great value for statistical analysis of various meteorological parameters.

- High resolution numerical simulations produce realistic orographic wind patterns. However, an in-depth investigation of a downslope windstorm reveals substansial sensitivity of the simulated surface winds to microphysical processes upstream of the mountain, through their influences on static stability.

- A new two-equation planetary boundary layer scheme, with a prognostic mixing length, captures well the magnitude of an extreme downslope windstorm.

Chapter 7

Onwards – yet more questions

The subtitle of this thesis, *Die zweite Aufgabe der theoretischen Meteorologie*, is taken from the 1904 *Das Problem der Wettervorhersage, betrachtet vom Standpunkte der Mechanik und der Physik* paper of Vilhelm Bjerknes. The work described in this thesis has to a large extent focused on atmospheric physics, how it is represented in atmospheric models, and consequently how these models can be used to gain a better understanding of the nature. An undertaking Bjerknes described as the second task of theoretical meteorology. Second indicates a *first*, and indeed Bjerknes describes the *erste Aufgabe* as well as the second one.

7.1 First task of theoretical meteorology

Numerical weather predictions are generated by integrating systems of differential equations forward in time. The equations are derived from the basic laws of physics and fluid motion. The initial state of this global modeling system is derived by merging observations from satellites, radio-sondes, and other sources, with the latest forecasting cycle. These measurements are taken all over the world, and over a certain period, usually the last six hours prior to the initiation time. This data assimilation methodology ensures that the initial state of the atmosphere, as simulated by the modeling system, is in close agreement with available observations, as well as being a solution to the system of differential equations.

The importance of data assimilation, albeit not called by that name at the time, was already realized by Vilhelm Bjerknes in early 1900s. In his 1904 paper Bjerknes expressed his vision and program for weather forecasting (Grønås, 2005). In this paper he states that “Based on the observations made, the first task of theoretical meteorology will then be to derive the clearest possible picture of the physical and dynamical state of the atmosphere at the time of the observations. This picture must be in a form that is appropriate to serve as a starting point for a weather prediction

according to rational dynamical-physical methods[1]". Bjerknes realized that this task was not possible at the time, essential data was missing from over the oceans and upper-air observations were lacking as well.

7.1.1 Data assimilation

As stated by A. J. Simmons in his Vilhelm Bjerknes medal lecture at the EGU conference in Vienna in 2012: "The key to addressing Bjerknes's first task has been the development of data assimilation. Data assimilation provides a sequence of analyses of atmospheric and related oceanic and land-surface conditions. It uses information from the latest observations to adjust a background model forecast initiated from the preceding analysis in the sequence. The model carries information from earlier observations forward in time, and information is spread in space and from one variable to another by the model forecast and through the background-error structures used in the adjustment process. The set of observations may comprise many different types of measurement, each with its own accuracy and spatial distribution." Essentially, the core of any data assimilation system is to balance the observational and forecast uncertainty (cf. Fig. 7.1).

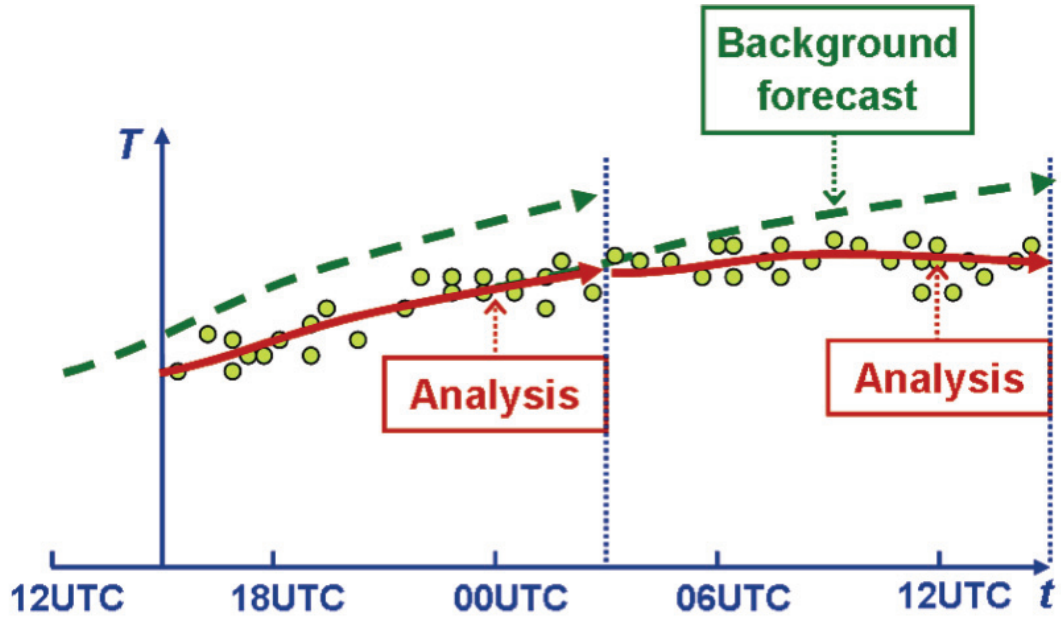

Figure 7.1: *To produce an estimate of the atmospheric state, data assimilation blends information from observations, short background forecast, estimates of observational and background errors, and dynamical relationships built into the representation of background errors. From Simmons (2012).*

[1] From the english translation of the Bjerknes 1904 paper, Bjerknes (2009).

Edward Lorenz argues in his 1982 paper that the Root Mean Square (RMS) difference curve (cf. Fig. 7.2) is the limit of the forecast improvement that is possible without reducing the day-1 forecast error, assuming that the model has realistic intrinsic error-growth characteristics. As can clearly be seen in Fig. 7.2 about half of

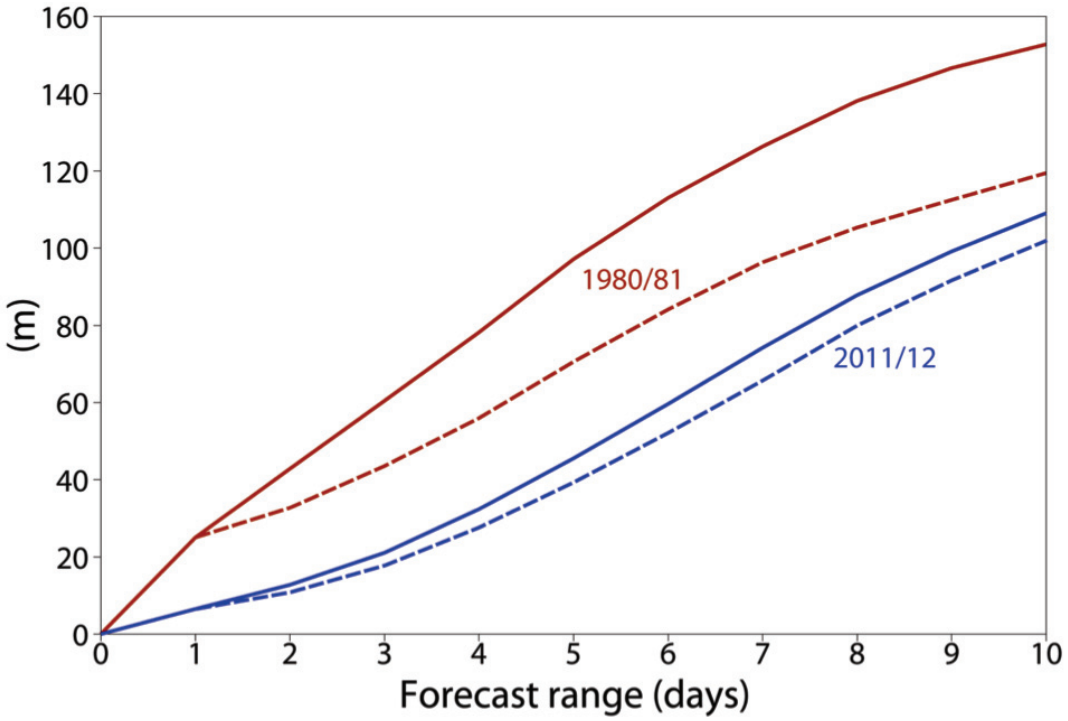

Figure 7.2: *Root Mean Square (RMS) error of the forecast (solid line) and RMS difference between successive daily forecasts (dashed lines) for the 500 hPa height for the period December to February in the extratropical northern hemisphere. Red lines are for 1980/81 and blue curves for 2010/11. From Simmons (2012).*

the ECMWF forecast improvements from 1980/81 to 2010/11 stems from improving the knowledge of the initial state of the atmosphere.

7.1.2 Potential of regional data assimilation

In recent years considerable advances have been made in data assimilation for regional models. Ready to use assimilation systems are now available for the WRF modeling system (e.g. DART[2], GSI[3] and WRFDA[4]), offering 3D-VAR, 4D-VAR, FDDA and EnKF methods. One can now also assimilate radiances data from satellites and/or ground based radars, although care must be taken when choosing which

[2]http://www.image.ucar.edu/DAReS/DART
[3]http://www.dtcenter.org/com-GSI/users
[4]http://www.mmm.ucar.edu/wrf/users/wrfda

channels should be used. One should also keep in mind that the quality of certain satellite data can be reduced if there is cloud cover. Global Positioning System (GPS) Radio Occultation (RO) data can provide high-resolution vertical profiles of refractivity, independent of cloud cover, and hence high-resolution profiles of temperature and humidity. Assimilation of this type of data has been shown to improve the operational forecasts of the Central Weather Bureau of Taiwan (Hong and Fong, 2012). In light of this, it would be a very interesting research task to investigate the potential of using data from the extensive GPS network in Iceland (cf. Fig. 3.2) to improve the atmospheric analysis, and consequently provide a better weather forecast.

7.2 Second task of theoretical meteorology

In the 1904 paper Bjerknes also describes the second task of theoretical meteorology as "...the second and most challenging task of theoretical meteorology will be to construct the pictures of the future states of the atmosphere from the picture of the current state of the atmosphere as a starting point, either according to the method outlined here, or according to a method of a similar kind[5]". The details of the second task were outlined in Lewis Fry Richardson's book *Weather prediction by numerical process* in 1922. The first numerical forecast, using an electronic computer, was then done by Charney, Fjörtoft and von Neumann in 1950 (Charney et al., 1950) The computer in question was named ENIAC and was the first general purpose computer ever built, a historical overview of this accomplishment can be found in Platzman (1979).

The methods used to tackle this task have continuously been improved upon to this day.

7.2.1 Terra Incognita

There are limitations that current one-dimensional planetary boundary layer (PBL) schemes face as the horizontal model resolution (Δ) approaches the scale, l, of the flux- and turbulent containing eddies. Current PBL schemes were simply not designed to be used when Δ and l are of the same order. This numerical region is termed "Terra Incognita" by Wyngaard (2004), and it is this region we now fast approach as the need for even higher horizontal resolution and more detailed model results is emerging.

The limits of running the WRF model below 1 km resolution was demonstrated in a recent study by Elíasson et al. (2011). In this study a comparison was made between measured and simulated in-cloud ice loading in E-Iceland. The simulated ice

[5]From the english translation of the Bjerknes 1904 paper, Bjerknes (2009)

loading was based on numerical data from the WRF model, describing the state of the atmosphere at high spatial and temporal resolution, ranging from 9 to 0.33 km. It is found that the model performance increases as the resolution is increased, especially when going from 3 km to 1 km, but only moderately when going from 1 km to 0.33 km.

A promising substitute to conventional PBL schemes is the 3D-TKE method, but flux issues need to be addressed and fixed (Rögnvaldsson et al., 2011) before this scheme can be used for real case applications.

7.2.1.1 Use of additional observations

The Elíasson et al. (2011) case study further shows that the results from the atmospheric model improve considerably when, in addition to the atmospheric analysis, the model is forced through nearby surface based observations of weather. This is especially important when the temperature is close to or just below 0°C as a small error in simulated temperature will strongly influence whether icing is taking place or not. Care must be taken when nudging the WRF model using only surface observations as the data may not be representative for the lowest part of the boundary layer in the case of low-level inversion.

As was pointed out in Jonassen et al. (2012), a clear advantage of using data from Unmanned Aerial Systems (UAS) rather than from automatic weather stations (AWS) is that it provides observations not only from near the surface, but also from an atmospheric column further aloft. Thereby, one can avoid several issues connected to e.g. the assimilation of only surface temperature observations, which are known to be especially problematic, e.g. Reen and Stauffer (2010).

Lack of observational turbulence data has also often been stated as a hindrance to improving PBL schemes (e.g. Lorsolo et al. (2010) and references therein). In this paper Lorsolo et al. describe a new method to assess the distribution of the turbulent energy in a hurricane using airborne Doppler measurements. The authors point out that when combined with surface wind and thermodynamic information, an accurate assessment of the TKE in the PBL could be used to estimate other important parameters, such as eddy diffusivity and dissipation, necessary to evaluate model parameterization schemes.

The kind of observations described in Lorsolo et al. require quite expensive observational platforms and can only be carried out by large governmental agencies such as NOAA. Another, and a much cheaper, approach was introduced by Reuder and Jonassen (2012). Here, the unmanned aerial system SUMO (Reuder et al., 2009), equipped with a miniaturized 5-hole probe, was used to observe the 3D turbulence field within a wind farm in Denmark. Granted, one cannot expect the SUMO, weighing less than one kilogram, to operate within a tropical cyclone. This platform has however proved quite useful in a number of field experiments in

Iceland, Norway, and Spitsbergen (e.g. Reuder et al. (2012); Jonassen et al. (2012)).

We must keep in mind that fluxes of momentum and heat are necessary lower boundary conditions for any PBL scheme. Hence, even if we have a "perfect" PBL scheme that could handle equally well sub filter-scale turbulences at a 10 km grid as on a 10 m grid, we would still be riddled with errors in the model results if the lower boundaries are not of equal quality. Hence, the quality of the land surface model is becoming ever greater as well as the accuracy of the underlying landuse characteristic and topography data. The quality and availability of the latter, i.e. the altitude data, has greatly improved with the emerging of the ASTER[6] (and most recently the ASTER2) data sets that has a 25 meter resolution and spans the globe from 85°south to 85°north.

Observations of hydrometeors are necessary to determine why the model does not capture lee side precipitation (i.e. the REX cases). Two theories were proposed in Rögnvaldsson et al. (2007a), but neither one can be verified or refuted without additional observations. This is needed in order to be able to see what parts of the model need to be improved upon. Recent research (Nicoll and Harrison, 2012) indicate that it may be possible to observe these cloud properties using relatively cheap and lightweight sensors, either via radio-sondes or deployed on UAS's. If proven useful, this kind of observations could become an option compared to expensive remote sensing measurements that can also be used for model evaluation and data assimilation. Han et al. (2012) use observations from a space-borne radiometer and a ground-based precipitation profiling radar to study the impact different cloud microphysics schemes in the WRF model have on the simulated microwave brightness temperature, radar reflectivity, and Doppler velocity, during a winter storm in California. Four microphysics schemes were tested, each having unique assumptions of particles size distributions, number concentrations, shapes, and hydrometeor fall speeds. These information are implemented into a satellite simulator and customized calculations for the radar are performed to ensure consistent representation of precipitation properties between the microphysics schemes and the radiative transfer models. This methodology of integrating an atmospheric model with a forward radiative transfer model has recently been used to evaluate model simulations and to improve model microphysics schemes (e.g. Matsui et al. (2009); Han et al. (2010); Li et al. (2010); Shi et al. (2010)). It is also one of the key components in algorithm development to retrieve or assimilate remote sensing data (Han et al., 2012).

[6] http://asterweb.jpl.nasa.gov/gdem.asp

7.3 Modeling of volcanic ash dispersion

Contrary to the data assimilation methodology used for global (and in some cases regional) weather forecasting, predictions of ash cloud dispersion make very limited use of observations far from the source of the eruption. The dispersion forecast starts at the source, e.g. an eruption column in Iceland, and the material is then transported along the wind track. Under normal weather conditions the atmospheric flow reaches Europe in a few days. During this time a variety of unknown natural processes affect the exact constituent and distribution of the ash cloud. Without the support of in-situ measurements, not only at the source (i.e. the erupting volcano), but also along the dispersion track, the simulated volcanic ash concentration will inevitably be too high as a consequence of the "safety first rule". This prediction technique needs to be improved by reducing the error that is generated during the propagation calculations.

The most important parameters used as input to the dispersion model, be it an Eulerian or Lagrangian one, are:

1. The scale of the eruption, including the erupted mass of ash.
2. The initial altitudes of the ash particles.
3. Eruption rate.
4. Grain size spectrum of the ash particles.

It should be stressed that in-situ and/or remote sensing observations at, or near, the source can improve the distribution forecast close to the erupting volcano (i.e. parameters 1 to 4 above). However, it is very difficult, if not impossible, to observe these parameters with adequate accuracy at the source, or even just to get the order of magnitude correct.

On the other hand, it is possible (up to a certain altitude) to observe parameters 2 and 4 (ash cloud height and grain size spectrum) downwind of the eruption using known and relatively simple techniques (Weber et al., 2012). When the eruption has been ongoing for some hours, and the ash cloud has been distributed some distance, these are the most important parameters to measure. The reason for this is twofold:

1. These parameters are advected with the atmospheric flow and are ultimately the parameters that affect air traffic safety.
2. Using observations, these parameters can be assimilated with the volcanic ash dispersion simulation, improving the ash distribution forecast.

As the eruption prolongs, and the volcanic ash is distributed over greater and greater distances it becomes necessary to observe parameters 2 and 4 over as much part of the affected area as possible.

A research project has been proposed to develop a new method, based on Kalman filtering, to assimilate measurements of volcanic ash density into a Eulerian dispersion model such as the Volcanic-WRF (Stuefer et al., 2012)[7]. The observations are to be collected in-situ from an airborne platform in the near-field of the crater (up to 200-300 km from the source). The objective is to generate more accurate forecasts than are available today where Lagrangian dispersion models are used to propagate the variables of the ash dispersion process for days without making corrections to the state variables, or model parameters, based on airborne measurements. The scientific value of this research project lies in the capability to predict and detect at any point in time with a high degree of accuracy the geographical boundaries where the concentration of volcanic ash exceeds the level that can be safely navigated by modern jet transport aircraft. For this purpose it is imperative that the measurements will be used in an optimal manner in order to correct the forecast variables and the model parameters where appropriate. Research done in other environmental areas, in particular in the Netherlands, has proven the value of applying certain types of Kalman filters for this purpose (Segers, 2002; Heemink and Segers, 2002). Hence this general approach is being proposed for the new research project focused on volcanic ash. The financial stakes are enormous as the disruption of air transport operations in Iceland has been very costly to the airlines and the tourism industry. It is also clear that this subject is of great interest to other European states that have experienced major disruptions of air transport due to volcanic ash emanating from volcanic eruptions in Iceland.

It should also be kept in mind that there is an actual possibility that, during an eruption, all international airports in Iceland may be closed, due to inaccurate ash distribution forecasts. The consequences of such airport, and airspace, closures could indeed proof dire.

[7]This version of WRF has been used to simulate the ash dispersion from the Mt. Eyjafjallajökull eruption in 2010 (Webley et al., 2012)

Bibliography

Andreae, M. O. and Rosenfeld, D., 2008. Aerosol cloud precipitation interactions. Part 1. The nature and sources of cloud-active aerosols. *Earth Science Reviews*, **89**: 13–41.

Arason, T., Rögnvaldsson, Ó. and Ólafsson, H., 2010. Validation of Numerical Simulations of Precipitation in Complex Terrain at high Temporal Resolution. *Hydrol. Res.*, **41**(3–4): 164–170.

Asai, T., 1965. A Numerical Study of the Air-Mass Transformation over the Japan Sea in Winter. *J. Meter. Soc. Japa.*, **43**: 1–15.

Bao, J. W., Michelson, S. A., Kantha, L. H. and Brown, J. W., 2008. Implementation of a Two–Equation Vertical Turbulent Mixing Scheme in a Mesoscale Atmospheric Model. NOAA Technical Memorandum OAR PSD–311. National Oceanic and Atmospheric Administration, Boulder, CO, 33 pp.

Berry, E. X. and Reinhardt, R. L., 1974. An Analysis of Cloud Drop growth by Collection: Part I. Double Distribution. *J. Atmos. Sci.*, **31**: 1814–1824.

Bjerknes, V., 1904. Das problem der wettervorhersage, betrachtet vom standpunkte der mechanik und der physik. *Meteorolog. Z.*, **21**: 1–7.

Bjerknes, V., 2009. The problem of weather prediction, considered from the viewpoints of mechanics and physics. *Meteorolog. Z.*, **18**(6): 663–667. Translated and edited by Volken E. and S. Bronnimann.

Bosart, L. F., 2003. Whither the Weather Analysis and Forecasting Process? *Weather and Forecasting*, **18**: 520–529.

Bougeault, P., Binder, P., Buzzi, A., Dirks, R., Houze, R., Kuettner, J., Smith, R., Steinacker, R. and Volkert, H., 2001. The map special observing period. *Bull. Amer. Meteor. Soc.*, **82**(3): 433–462.

Bright, D. R. and Mullen, S. L., 2002. The Sensitivity of the Numerical Simulation of the Southwest Monsoon Boundary Layer to the choice of PBL Turbulence Parameterization in MM5. *Wea. Forecasting*, **17**: 99–114.

Bromwich, D. H., Bai, L. and Bjarnason, G. G., 2005. High-resolution regional climate simulations over iceland using polar mm5. *Mon. Weather Rev.*, **133**(12): 3527–3547.

Charney, J. G. and Eliassen, A., 1949. A Numerical Method for predicting the Perturbations of the middle Latitude Westerlies. *Tellus*, **1**: 38–54.

Charney, J. G., Fjörtfoft, R. and Von Neumann, J., 1950. Numerical integration of the barotropic vorticity equation. *Tellus*, **2**(4): 237–254.

Chiao, S., Lin, Y.-L. and Kaplan, M. L., 2004. Numerical Study of the Orographic Forcing of Heavy Precipitation during MAP IOP-2B. *Mon. Weather Rev.*, **132**: 2184–2203.

Cotton, W. R., Bryan, G. and van den Heever, S. C., 2011. Chapter 4 - the parameterization or modeling of microphysical processes in clouds. G. B. William Cotton and S. van den Heever, editors, *Storm and Cloud Dynamics The Dynamics of Clouds and Precipitating Mesoscale Systems*, volume **99** of *International Geophysics*, pp. 87–142. Academic Press.

Déqué, M., Dreveton, C., Braun, A. and Cariolle, D., 1994. The ARPEGE/IFS atmosphere model: a contribution to the French community climate modelling. *C*limate Dynamics, **10**: 249–266.

Dudhia, J., 1989. Numerical study of convection observed during the winter monsoon experiment using a mesoscale two–dimensional model. *J. Atmos. Sci.*, **46**: 3077–3107.

Durran, D. R., 1990. Mountain Waves and Downslope Winds. W. Blumen, editor, *Atmospheric Processes Over Complex Terrain*, pp. 59–81. American Meteorological Society, Boston.

Elíasson, J., Rögnvaldsson, Ó. and Jónsson, T., 2009. Extracting Statistical Parameters of extreme Precipitation from a NWP Model. *Hydrol. Earth Syst. Sci.*, **13**: 2233–2240.

Elíasson, Á. J., Thorsteins, E., Ágústsson, H. and Rögnvaldsson, Ó., 2011. Comparison between simulations and measurements of in-cloud icing in test spans. *14th IWAIS (International Workshop on Atmospheric Icing of Structures) conference*. Chongqing, China. Extended abstract, 8 pages. Available on-line: http://www.wire1002.ch/fileadmin/user_upload/Major_events/WS_Nice_2011/-Spec._posters/ES1002_extended_abstract_Agustsson_ICING.pdf.

Feynman, R. P., Leighton, R. B. and L., S. M., 1963. The Feynman Lectures on Physics. Addison-Wesley Pub. Co.

Fletcher, N. H., 1965. The Physics of Rain Clouds. Cambridge University Press, Cambridge, first edition.

Giorgi, F. and Mearns, L. O., 1999. Introduction to special section: Regional climate modeling revisited. *J. Geophys. Res.*, **104**(D6): 6335–6352.

Grell, G. A., Dudhia, J. and Stauffer, D. R., 1995. A Description of the Fifth–Generation Penn State/NCAR Mesoscale Model (MM5). NCAR/TN–398+STR. National Center for Atmospheric Research, Boulder, CO, 107 pp.

Grønås, S., 2005. Vilhelm bjerknes vision for scientific weather prediction. *The Nordic Seas: an integrated perspective. Geophysical Monograph Series*, pp. 357–366. Am. Geophys. Union. 158.

Han, M., Braun, S. A., Matsui, T. and Williams, C. R., 2012. Evaluation of cloud microphysics schemes in simulations of a winter storm using radar and radiometer measurements. To appear in *J. Geophys. Res., Atmosphere*.

Han, M., Braun, S. A., Olson, W. S., Persson, P. O. G. and Bao, J.-W., 2010. Application of TRMM PR and TMI Measurements to Assess Cloud Microphysical Schemes in the MM5 for a Winter Storm. *J. Appl. Meteor. Climatol.*, **49**(6): 1129–1148.

Heemink, A. W. and Segers, A. J., 2002. Modeling and prediction of environmental data in space and time using kalman filtering. *Stochastic Environmental Research and Risk Assessment (SERRA)*, **16**(3): 225–240.

Hong, J.-S. and Fong, C.-T., 2012. Highlights of the Operational WRF-Based Numerical Prediction System at Central Weather Bureau of Taiwan. *13th Annual WRF Users' Workshop*. Boulder, Colorado. Available on-line: http://www.mmm.ucar.edu/wrf/users/workshops/WS2012/ppts/2.4.pdf.

IPCC, 2007. Stationary and quasi-stationary eddies in the extratropical troposphere: theory. Solomon, S., D. Qin, M. Manning, Z. Chen, M. Marquis, K.B. Averyt, M. Tignor and H.L. Miller, editor, *Contribution of Working Group I to the Fourth Assessment Report of the Intergovernmental Panel on Climate Change*. Cambridge University Press, Cambridge, United Kingdom and New York, USA.

Jonassen, M. O., Ólafsson, H., Ágústsson, H., Rögnvaldsson, Ó. and Reuder, J., 2012. Improving high resolution numerical weather simulations by assimilating data from an unmanned aerial system. *Mon. Weather Rev.*, **140**(11): 3734–3756. Available on-line: http://journals.ametsoc.org/doi/abs/10.1175/MWR-D-11-00344.1journalCode=mwre.

Kristjánsson, J. E. and McInnes, H., 1999. The impact of Greenland on cyclone evolution. *Q. J. R. Meteorol. Soc.*, **125**: 2819–2834.

Li, X., Tao, W.-K., Matsui, T., Liu, C. and Masunaga, H., 2010. Improving a spectral bin microphysical scheme using trmm satellite observations. *Q. J. R. Meteorol. Soc.*, **136**(647): 382–399.

Lorenz, E. N., 1982. Atmospheric predictability experiments with a large numerical model. *Tellus*, **34**(6): 505–513.

Lorsolo, S., Zhang, J. A., Marks, F. and Gamache, J., 2010. Estimation and mapping of hurricane turbulent energy using airborne doppler measurements. *Mon. Weather Rev.*, **138**(9): 3656–3670.

Marshall, J. S. and Palmer, W. M., 1948. The Distribution of Raindrops with Size. *J. Atmos. Sci.*, **5**: 165–166.

Matsui, T., Zeng, X., Tao, W.-K., Masunaga, H., Olson, W. S. and Lang, S., 2009. Evaluation of long-term cloud-resolving model simulations using satellite radiance observations and multifrequency satellite simulators. *J. Atmos. Oceanic Technol.*, **26**: 1261–1274.

Meyers, M. P., DeMott, P. J. and Cotton, W. R., 1992. New Primar Ice-Nucleation Parameterization in an Explicit Cloud Model. *J. Appl. Meteor.*, **31**: 708–721.

Nakićenović, N., Alcamo, J., Davis, G., de Vries, B., Fenhann, J., Gaffin, S., Gregory, K., Grübler, A., Jung, T. Y., Kram, T., Lebre La Rovere, E., Michaelis, L., Mori, S., Morita, T., Pepper, W., Pitcher, H., Price, L., Riahi, K., Roehrl, A., Rogner, H. H., Sankovski, A., Schlesinger, M., Shukla, P., Smith, S., Swart, R., van Rooijen, S., Victor, N. and Dadi, Z., 2000. IPCC Special Report on Emissions Scenarios (SRES). Cambridge University Press, UK.

Nicoll, K. and Harrison, R. G., 2012. Cloud detection using disposable airborne sensors. *Geophysical Research Abstracts*, volume **14**. Vienna, Austria. Available on-line: http://meetingorganizer.copernicus.org/EGU2012/EGU2012-8218.pdf.

Nolan, P., Lynch, P. and Sweeney, C., 2012. Simulating the future wind energy resource of Ireland using the COSMO-CLM model. *Wind Energy*. Available on-line: http://dx.doi.org/10.1002/we.1554.

Ólafsson, H., 2000. Comment les Montagnes Ralentissent-Elles le Vent? *La Mètèorologie*, **8**(31): 19–24.

Ólafsson, H., 2003. Forecasting winds in the vicinity of mountains. Tech.rep., The Eumetcal Library. Available on the web: http://www.eumetcal.org/intralibrary/open_virtual_file_path/i204n4542t/forecasting_winds_in_the_vicinity_of_mountains.ppt.

Ólafsson, H. and Bougeault, P., 1997. The effect of rotation and surface friction on orographic drag. *J. Atmos. Sci.*, **54**: 193–210.

Platzman, G. W., 1979. The ENIAC Computations of 1950-Gateway to Numerical Weather Prediction. *Bull. Amer. Meteor. Soc.*, **60**: 302–312.

Qian, J.-H., Seth, A. and Zebiak, S., 2003. Reinitialized versus continuous simulations for regional climate downscaling. *Mon. Weather Rev.*, **131**(11): 2857–2874.

Reen, B. and Stauffer, D., 2010. Data assimilation strategies in the planetary boundary layer. *Boundary-Layer Meteorology*, pp. 1–33–33.

Reisner, J., Rasmussen, R. M. and Bruintjes, R. T., 1998. Explicit forecastin of supercooled liquid water in winter storms using the MM5 mesoscale model. *Q. J. R. Meteorol. Soc.*, **124B**: 1071–1107.

Reuder, J., Ablinger, M., Ágústsson, H., Brisset, P., Brynjólfsson, S., Garhammer, M., Jóhannesson, T., Jonassen, M., Kühnel, R., Lämmlein, S., Lange, T., Lindenberg, C., Malardel, S., Mayer, S., Müller, M., Ólafsson, H., Rögnvaldsson, Ó., Schäper, W., Spengler, T., Zängl, G. and Egger, J., 2012. Flohof 2007: an overview of the mesoscale meteorological field campaign at hofsjökull, central iceland. *Meteorol. Atmos. Phys.*, **116**: 1–13.

Reuder, J., Brisset, P., Jonassen, M., Müller, M. and Mayer, S., 2009. The small unmanned meteorological observer sumo: A new tool for atmospheric boundary layer research. *Meteorolog. Z.*, **18**(2): 141–147.

Reuder, J. and Jonassen, M. O., 2012. Turbulence measurements in a wind park with the Micro-UAS SUMO. *Geophysical Research Abstracts*, volume **14**. Vienna, Austria. Available on-line: http://meetingorganizer.copernicus.org/EGU2012/EGU2012-3471.pdf and http://presentations.copernicus.org/EGU2012-3471_presentation.pdf.

Richardson, L., 1922. Weather prediction by numerical process. University Press.

Rogers, R. and Yau, M., 1989. A short course in cloud physics. International series in natural philosophy. Pergamon Press.

Rögnvaldsson, Ó., 2011. Search and Rescue Software, Weather Prediction System assists Humanitarian Aid. *Meteorological Technology International*, pp. 76–78.

Rögnvaldsson, Ó., Bao, J.-W., Ágústsson, H. and Ólafsson, H., 2011. Downslope Windstorm in Iceland - WRF/MM5 Model Comparison. *Atmospheric Chemistry and Physics*, **11**: 103–120.

Rögnvaldsson, Ó., Bao, J.-W. and Ólafsson, H., 2007a. Sensitivity Simulations of Orographic Precipitation with MM5 and Comparison with Observations in Iceland during the Reykjanes EXperiment. *Meteorolog. Z.*, **16**(1): 86–98.

Rögnvaldsson, Ó., Crochet, P., and Ólafsson, H., 2004. Mapping of Precipitation in Iceland using Numerical Simulations and Statistical Modeling. *Meteorolog. Z.*, **13**(3): 209–219.

Rögnvaldsson, Ó., Jónsdóttir, J. F., and Ólafsson, H., 2007b. Numerical Simulations of Precipitation in the Complex Terrain of Iceland – Comparison with Glaciological and Hydrological Data. *Meteorolog. Z.*, **16**(1): 71–85.

Rögnvaldsson, Ó., Jónsdóttir, J. F., and Ólafsson, H., 2010. Dynamical Downscaling of Precipitation in Iceland 1961-2006. *Hydrol. Res.*, **41**(3–4): 153–163.

Rögnvaldsson, Ó. and Ólafsson, H., 2005a. Numerical simulations of the climatology of winds in the complex terrain of Iceland. Proc. Int. Conf. Alp. Meteorol. (ICAM), p. 4. Available on-line: http://www.map.meteoswiss.ch/mapdoc/icam2005/pdf/poster-sesion-e/E39.pdf.

Rögnvaldsson, Ó. and Ólafsson, H., 2005b. The response of precipitation to orography in simulations of future climate. Proc. Int. Conf. Alp. Meteorol. (ICAM), p. 4. Available on-line: http://www.map.meteoswiss.ch/mapdoc/icam2005/pdf/poster-sesion-d/D33.pdf.

Rögnvaldsson, Ó., Ágústsson, H. and Ólafsson, H., 2011. WRFLES – A system for high-resolution limited area numerical simulations. Tech.Rep. 1, Institute for Meteorological Research. Available on-line: ftp://betravedur.is/pub/wrf/icam2011/UniRes_WRFLES.pdf.

Schultz, P., 1995. An Explicit Cloud Physics Parameterization for Operational Numerical Weather Prediction. *Mon. Weather Rev.*, **123**: 3331–3343.

Segers, A., 2002. Data assimilation in atmospheric chemistry models using Kalman filtering. Ph.D. thesis. Available on-line: http://resolver.tudelft.nl/uuid:113b6229-c33a-4100-93be-22e1c8912672.

Shi, J. J., Tao, W.-K., Matsui, T., Hou, A., Lang, S., Peters-Lidard, C., Jackson, G., Cifelli, R., Rutledge, S. and Petersen, W., 2010. Microphysical Properties of the January 20-22 2007 Snow Events over Canada: Comparison with in-situ and Satellite Observations. *J. Appl. Meteor. Climatol.*, **49**: 2246–2266.

Simmons, A. J., 2012. Vilhelm Bjerknes's "First task of theoretical meteorology": Assimilation of observational data for atmospheric monitoring and forecasting. *Geophysical Research Abstracts*, volume **14**. Vienna, Austria. Available on-line: http://meetingorganizer.copernicus.org/EGU2012/EGU2012-14441.pdf and http://presentations.copernicus.org/EGU201214441_presentation.pdf.

Skamarock, W. C., Klemp, J. B., Dudhia, J., Gill, D. O., Barker, D. M., Duda, M. B., Huang, X.-Y., Wang, W. and Powers, J. G., 2008. A Description of the Advanced Research WRF Version 3. NCAR Technical Note, NCAR/TN–475+(STR). National Center for Atmospheric Research, Boulder, CO, 113 pp.

Smith, R. B., 1989. Hydrostatic Airflow over Mountains, volume 31 of *Advances in Geophysics*. Academic Press.

Stensrud, D. J., 2007. Parameterization Schemes. Cambridge University Press, Cambridge, first edition.

Stoelinga, M. T., Hobbs, P. V., Mass, C. F., Locatelli, J. D., Colle, B. A., Houze, Jr., R. A., Rangno, A. L., Bond, N. A., Smull, B. F., Rasmussen, R. M., Thompson, G. and Colman, B. R., 2003. Improvement of Microphysical Parameterization through Observational Verification Experiment. *Bull. Amer. Meteor. Soc.*, **84**: 1807–1826.

Stuefer, M., Freitas, S. R., Grell, G., Webley, P., Peckham, S. and McKeen, S. A., 2012. Inclusion of Ash and SO_2 emissions from volcanic eruptions in WRF-CHEM: development and some applications. *Geoscientific Model Development Discussions*, **5**(3): 2571–2597.

Stull, R. B., 1988. An Introduction to Boundary Layer Meteorology. Atmospheric Sciences Library. Kluwer Academic Publisher, London.

Stull, R. B., 2006. The Atmospheric Boundary Layer. J. M. Wallace and P. V. Hobbs, editors, *Atmospheric Science. An Introductory Survey*, volume 92 of *International Geophysics Series*, pp. 375–418. Elsevier, London.

Thorsteinsson, T. and Björnsson, H., editors, 2012. Climate Change and Energy Systems: Impacts, Risks and Adaptation in the Nordic and Baltic countries. Nordic Council of Ministers, Copenhagen.

Walko, R. L., Cotton, W. R., Meyers, M. P. and Harrington, J. Y., 1995. New RAMS cloud microphysics parameterization. Part I: The single–moment scheme. *Atmos. Res.*, **38**: 29–62.

Wallace, J. M. and Hobbs, P. V., 2006. Atmospheric Science: An Introductory Survey. Academic Press, New York.

Warner, T. T., 2011. Numerical Weather and Climate Prediction. Cambridge University Press, Cambridge, first edition.

Warner, T. T., Peterson, R. A. and Treadon, R. E., 1997. A Tutorial on Lateral Boundary Conditions as a Basic and Potentially Serious Limitation to Regional Numerical Weather Prediction. *Bull. Amer. Meteor. Soc.*, **78**: 2599–2617.

Weber, K., Eliasson, J., Vogel, A., Fischer, C., Pohl, T., van Haren, G., Meier, M., Grobéty, B. and Dahmann, D., 2012. Airborne in-situ investigations of the Eyjafjallajökull volcanic ash plume on Iceland and over north-western Germany with light aircrafts and optical particle counters. *Atmospheric Environment*, **48**: 9–21.

Webley, P. W., Steensen, T., Stuefer, M., Grell, G., Freitas, S. and Pavolonis, M., 2012. Analyzing the Eyjafjallajökull 2010 eruption using satellite remote sensing, lidar and WRF-Chem dispersion and tracking model. *J. Geophys. Res.*, **117**.

Wyngaard, J. C., 2004. Toward Numerical Modeling in the "Terra Incognita". *J. Atmos. Sci.*, **61**: 1816–1826.